The role of miR-320d in cervical cancer cell lines under basal conditions and after exposure to ionizing radiation

Unn Beate Salberg

Master thesis in Molecular Bioscience

UNIVERSITY OF OSLO

June 2016

Year: 2016

The role of miR-320d in cervical cancer cell lines under basal conditions and after exposure to ionizing radiation

Author: Unn Beate Salberg

http://www.duo.uio.no/

Press: Reprosentralen, University of Oslo

Acknowledgements

The present work was carried out in the Clinical Radiation Biology group at the Department of Radiation Biology, Institute for Cancer Research, Norwegian Radium Hospital, Oslo University Hospital from April 2015 to June 2016.

First, I would like to thank my two supervisors, Malin Lando and Heidi Lyng, for all your guidance and for always being available to answer my questions. Our discussions always make things look brighter, and help me gain confidence in myself. I highly appreciate how much time you have dedicated to helping me during this thesis, and especially towards the end. A special thanks to Eva-Katrine Aarnes for spending hours on teaching me most of what I've learned in the laboratory during this period. I would also like to thank the whole research group for including me and for instantly making me feel welcome, and the Department of Radiation Biology for the very good social environment, both inside and outside the lab. You have all contributed to my desire to continue doing research.

The company of Nikoline Rasmussen and Dhaksshaginy Rajalingam, my fellow students and closest friends for five years, has been invaluable. Your achievements and good results have inspired me since the day we first met. Thank you for all academic discussions and for all waffles dates, workouts and other fun we've had outside university. I would also like to thank my fellow master students at the department, Torleif Tollefsrud Gjølberg and Tine Raabe, for good company in the lab.

I would like to thank all of my friends for all the fun we've had together as students. A special thanks to Silje Wilhelmsen, my best friend for 21 years, for being there when I need you the most. I would also like to thank my whole family for always supporting me, especially my parents Randi and Jens Anders, and my lovely little sister Birgitte.

Oslo, June 2016

Unn Beate Salberg

Abstract

Cervical cancer is the second most common female specific cancer on a global basis. Radiation therapy is commonly given as treatment when the cancer has progressed to advanced stages, but does also cause damage to normal tissue and can cause severe side-effects. Hence, a better understanding of cellular responses to radiation to improve the therapy is needed.

The chromosomal region 13q12.11-q21.1 is frequently lost in cervical cancer, and tumors with loss of this region are found to be more resistant to chemoradiotherapy than tumors without loss[1]. The resistance results in poor treatment outcome and it is therefore of great interest to distinguish between good and poor responders of radiation therapy in order to give a more personalized treatment. Of the 16 miRNAs located within this 13q region, miR-320d located at 13q14.11 was selected for further studies to better understand why loss corresponds with chemoradioresistance.

The cervical cancer cell lines HeLa and SiHa were used as model systems and miR-320d was overexpressed by transiently transfecting the cell lines with miR-320d mimics. A method for analyzing the expression of miR-320d by RT-qPCR was established in order to verify the overexpression. Additionally, the transfection duration was tested and compared with the cell doubling time. To investigate the biological role of miR-320d, phenotypical changes in cell survival, cell cycle distribution and apoptosis were studied using clonogenic assay and flow cytometry. A potential role of miR-320d in radioresistance was further explored by irradiating cells with 2 Gy and 4 Gy before running clonogenic assay.

Transfection was considered successful with an average miR-320d upregulation of 18 800x in SiHa cells and 10 900x in HeLa cells. The half-life of miR-320d in cells transfected with miR-320d mimics was found to be 44 hours for HeLa cells and 56 hours for SiHa cells. The respective cell doubling times were calculated to be 19 hours and 26 hours. A decrease in survival was observed in SiHa cells transfected with miR-320d mimics compared to the negative control (p=0.009), but not in HeLa cells. Radiosensitivity was tested by irradiating the cells with 2 Gy and 4 Gy, but increased radiosensitivity after upregulation of miR-320d was not seen in any of the cell lines. Neither were any differences observed in cell cycle distribution or apoptosis between mimic-treated and negative control cells for any of the cell lines.

In conclusion, miR-320d seems to contribute to decreased cell survival when overexpressed, and might also be involved in regulating other processes related to cancer by interaction with other miRNAs.

Abbreviations

Abbreviation	Description
bp	Base pairs
cDNA	Complementary DNA (deoxyribonucleic adid)
CIN	Cervical intraepithelial neoplasia
CNV	Copy number variation
DMEM	Dulbecco's Modified Eagle's Medium
dsDNA	Double-stranded DNA
dUTP	Deoxyuridine triphosphate
FBS	Fetal bovine serum
Gy	Gray
HPV	Human papilloma virus
miRNA	Micro RNA (ribonucleid acid)
mL	Milliliter
nM	Nanomolar
Nm	Nanometer
PBS	Phosphate buffered saline
PE	Plating efficiency
miRISC	Micro RNA-induced silencing complex
RT-qPCR	Real-time quantitative PCR (polymerase chain reaction)
SD	Standard deviation
SF	Survival fraction
ssDNA	Single-stranded DNA
TdT	Terminal deoxynucleotidyl transferase
TUNEL	Terminal deoxynucleotidyl transferase dUTP nick end labeling
w/v	Weight/volume
µg	Microgram
µL	Microliter
µM	Micromolar

Table of Contents

1 Introduction and aims

Cancer is a collection of more than 100 related diseases recognized by abnormal and uncontrolled cell growth[2]. Causes for this are loss of control of the system regulating cell growth, proliferation and cell death. Such regulation occurs at several different levels, included in these are the post-transcriptional regulation mechanisms mRNA degradation control and translation control[3].

On a global basis, cervical cancer is the fourth most common incident site of cancer among women and the second most common incident site of female specific cancer[4]. There are about 300 new cases of cervical cancer in Norway every year[5]. Treatment of cervical cancer depends on the tumor stage, but for locally advanced stages, radiotherapy combined with chemotherapy is chosen[6]. Patients with locally advanced cervical cancer respond differently to their treatment, even though they have "identical" tumors considering tumor type, size, and stage. One out of three patients is failing treatment, and they will have relapse and show progressive disease within 5 years after diagnosis. The rest of the patients will have disease control, but a problem is the serious side effects the therapy causes to other organs located in the pelvis. It is therefore a need for understanding the underlying biology leading to chemoradioresistance.

Almost all cases of cervical cancer are related to viral infections from high-risk human papillomavirus (HR-HPV), and 70 % of these are caused by HPV16 and HPV18[7]. HR-HPV encodes oncoproteins which target and inactivate essential cell cycle host proteins. However, HR-HPV infection and oncoprotein expression are not necessarily sufficient to lead to development of cervical cancer[8]. Other factors may also be involved, such as the small non-coding RNAs called microRNAs (miRNA). MiRNAs are a small group of non-coding RNAs which have been found to frequently be located at fragile sites and places in the genome related to cancer[9]. However, little research is done on miRNAs in cervical cancer.

In 2009, Lando et al. performed analysis of gene dosage, expression and ontology in a cohort of locally advanced cervical cancers to detect driver genes associated with poor outcome after chemoradiotherapy[1]. Among the findings were genetic alterations on chromosome 13q corresponding with poor outcome for patients with loss in this region. The loss seems to cause an aggressive phenotype, and miRNAs located within this region are therefore of interest to

study, as they might be involved in driving the cancer towards a more aggressive phenotype with increased chemoradioresistance.

To better understand the impact miRNA regulation has on the cells phenotype, a miRNA within the lost 13q region was selected for further studies. To upregulate the expression of a certain miRNA, cells can be transfected with a sequence resembling the chosen miRNA, called a miRNA mimic. The miRNA expression can then be measured using quantitative RT-PCR. Functional miRNA studies have not previously been done in our research group and it was therefore necessary to establish methods, both for miRNA upregulation by the use of mimics and for RT-qPCR analysis of miRNA expression in cell lines. Phenotypic traits of interest were cell survival, cell cycle distribution, induction of apoptosis and radiosensitivity of the cells. These features were decided to be studied by the use of flow cytometry and clonogenic assay.

The overall aim of this study was to better understand why some patients are poor responders of chemoradiotherapy, while others respond well. Insight into this may result in an improved and more personalized treatment for these patients. The more specific aims of the study can be divided into methodological- and biological aims:

Methodological aims

- Establish methods using RT-qPCR for analyzing miR-320d expression before and after upregulation with miRNA mimics. This included studying transfection duration in relation to the cellular doubling time.

Biological aims

- Investigate the cell survival after upregulation of miR-320d by performing clonogenic assays
- Investigate whether miR-320d affect the cell survival after ionizing radiation
- Examine whether the cell cycle distribution is changed in the model system after miR-320d is upregulated
- Study the fraction of apoptotic cells after upregulation of miR-320d

2 Background

2.1 Cervical cancer

The uterine cervix is located in the lower part of the uterine and is the opening into the uterus. The cervix consists of two types of epithelial cells, where squamous cells are located in the outermost part (squamous epithelium) and glandular cells are located in the innermost part (columnar epithelium) (Figure 2.1). Cervical carcinoma is a collective term used for various histological variants of cancers in the cervix. Most precancerous and cancerous cellular changes originate from the transition zone of the two epithelial cell types. Squamous cell carcinoma originates from the squamous epithelium and represents about 70-80 % of all cases. Adenocarcinoma arises from the columnar epithelium and is the second most common variant with about 10-15 % of all cases[10-11].

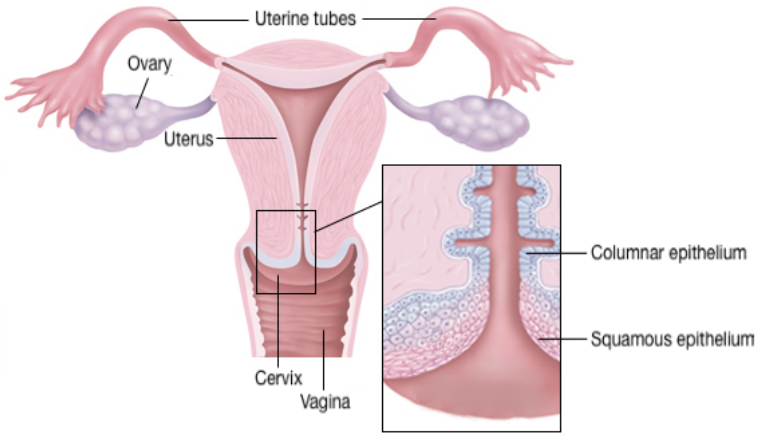

Figure 2.1: Female reproductive system and the epithelial cells of cervix. Figure adapted from Harvard Health[12] (edited version).

2.1.1 Staging

Precancerous lesions of the cervix are described as cervical intraepithelial neoplasia (CIN). CIN I display mild dysplastic changes in cervical epithelium, and this stage is a mixture of low risk and high risk HPV. Those with high risk HPV are the ones most likely to progress further into CIN II and III, which are associated with moderate dysplasia and severe dysplasia or carcinoma in situ[13], respectively. CIN III is almost exclusively associated with high risk HPV variants such as type 16 and 18. In contrast to CIN I patients, CIN II and III patients require treatment. Once

the lesions become invasive, the patient is diagnosed with cervical cancer. The cancer can be staged according to the International Federation of Gynecology and Obstetrics (FIGO) system, which include stages from 1, where the cancer is confined to cervix, to stage 4, where the cancer has spread from pelvis to distant organs of the body[14]. CIN III is considered as the additional stage 0. Patients with stage 1b to 4a are treated with radiotherapy[15], which involves both external and internal radiation (brachytherapy).

2.2 Central dogma

The central dogma of molecular biology describe the possible ways flow of information can occur within biological systems[16]. Three transfers of information are the most commonly occurring, and these include DNA to DNA (replication), DNA to RNA (transcription) and RNA to protein (translation) (Figure 2.2). All these processes are believed to take place in most cells. The processes following extraction of information stored within DNA can be regulated at many different levels, and thereby affect the cell phenotype, which is the traits or characteristics of the cell. Additionally, RNA can be made into DNA by a process called reverse transcription. The resulting DNA molecules are called complementary DNA (cDNA).

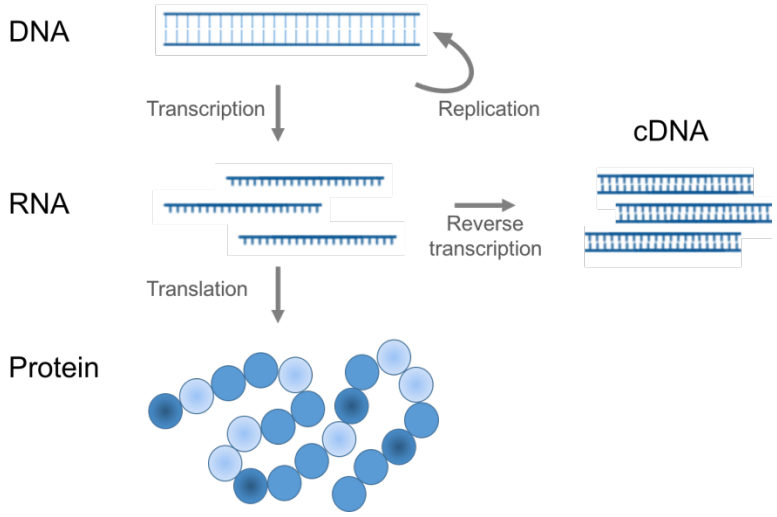

Figure 2.2: Transfer of information from DNA via RNA to protein, and the more special case where RNA is reverse-transcribed into cDNA.

2.3 Cell cycle

When a cell proliferates and divides into two daughter cells, it goes through a sequence of stages: G_1, S, G_2 and M phase[2] (Figure 2.3). The three first ones are together called interphase and consist of two gap phases (G_1 and G_2) and a phase where DNA synthesis occurs (S-phase). The fourth phase, M phase, is where the cell goes through partitioning to produce the two daughter cells. This phase includes the mitosis and cytokinesis.

G_1 is the phase of the cell cycle where the cell is dependent on growth factors to proliferate. After a control point called the G_1 checkpoint, or the restriction point, the cell is no longer dependent on external growth signals, but will be irreversibly committed to progress through the cell cycle. A special state called G_0 can be entered from G_1, and is a resting period where the cell can remain inactive for a long period of time. This phase is seen as "outside" the cell cycle.

S phase is when the entire DNA in the cell is duplicated. In the G_2 phase, the main task of the cell is to grow in mass, so that it is prepared for the division. Mitosis is when the duplicated chromosomes of the cell are separated into two nuclei, and involves further subdivisions. Cytokinesis is when the cytoplasm is divided into two separate daughter cells.

2.3.1 Regulation of the cell cycle

Distinct checkpoints control the progression through the cell cycle, avoiding the cell to divide unless the environment is favorable. In addition to set the point for where the cell is no longer dependent on mitogens, the G_1 checkpoint controls for damaged DNA synthesized in the S phase[2]. The G_2 checkpoint also controls for damaged or unreplicated DNA, and causes cell cycle arrest if the S phase is not completed correctly. The M checkpoint controls whether the chromosomes are correctly attached to the apparatus (spindle apparatus) responsible for separating it into their new nuclei.

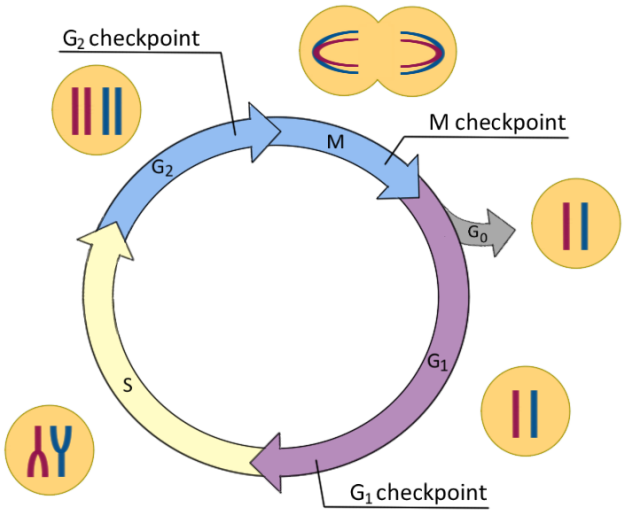

Figure 2.3: G_1 and G_2 are gap phases of the cell cycle. S phase is when the DNA is synthesized and M phase is when mitosis and cytokinesis occur. The checkpoints controlling DNA damage (G_1 and G_2), unreplicated DNA (G_2) and the spindle apparatus (M) are marked in their respective cell cycle phases.

2.4 Cancer development

If cell cycle control is in some way lost or altered, the cell can start to grow in an uncontrolled manner and become a cancer cell. Abnormal cell behavior will usually result in a controlled mechanism of cell death called apoptosis, which occurs when cells have too much damage to continue to divide[2]. Downregulation of pro-apoptotic genes or upregulation of anti-apoptotic genes can cause avoidance of this mechanism and is one of the most important hallmarks of cancer[17].

Carcinogenesis is the process where a tumor is developed from a normal cell (Figure 2.4). The normal cell can be exposed to one or more factors contributing to altered gene regulation resulting in carcinogenesis. These factors can be chemicals, radiation or virus infections, or genetic changes that occur by chance. If the genetic alteration is not repaired, the cell can become malignant and form daughter cells carrying the same damage. As soon as the cell first has got a mutation, the cell will become more prone to additional mutations, and what started as one single malignant cell will, by clonal expansion, proliferate into a malignant lesion containing multiple genetic alterations.

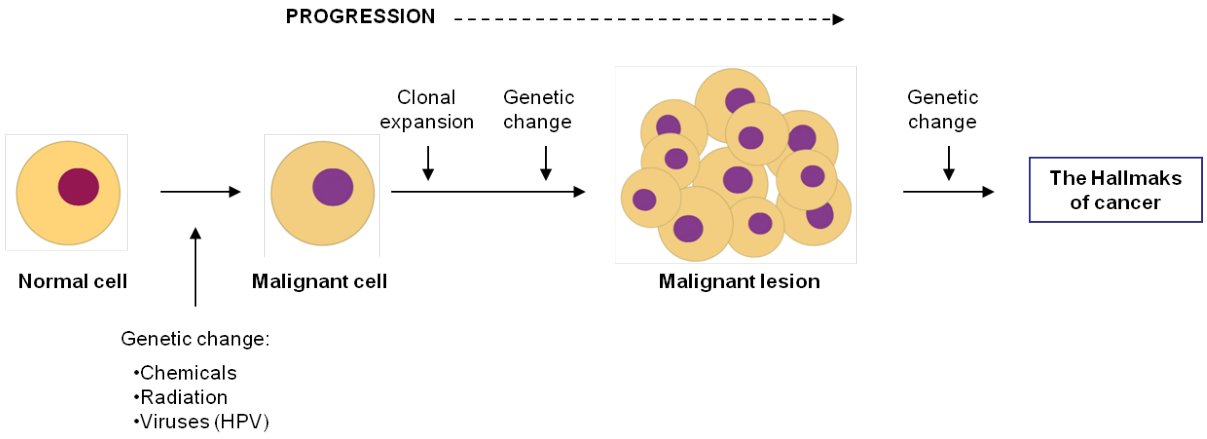

Figure 2.4: Transformation from a normal cell to a malignant cell and further progression into a malignant lesion

Genetic changes may include copy number variations (CNVs), which are deletions or duplications of parts of the genome, and point mutations, which are deletions, insertions or substitutions of a single nucleotide. These changes, together with epigenetic alterations and microRNAs (miRNAs), are the most common ways of gene regulation.

During the multistep progression of the tumor development, a variety of different characteristics are acquired, termed "the Hallmarks of Cancer"[17] (Figure 2.5). The traits considered in this thesis are resisting cell death (avoiding apoptosis), sustaining proliferative signaling and enabling replicative immortality (avoiding cell cycle arrest).

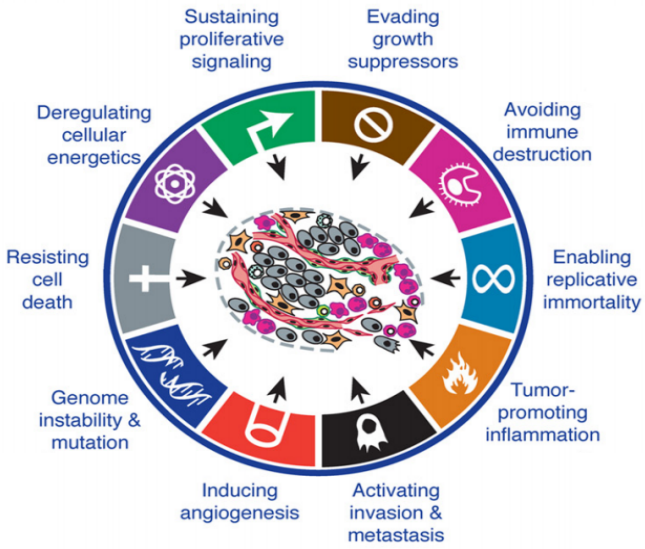

Figure 2.5: The Hallmarks of Cancer by Douglas Hanahan and Robert A. Weinberg (2011)[17].

2.4.1 HPV in cancer development

Human papillomaviruses (HPV) are non-enveloped DNA viruses with a genome size of approximately 8 kb[18], with more than 170 different variants existing[19]. The genome encodes six proteins early in the life-cycle (E1, E2, E4, E5, E6 and E7) and two proteins late (L1 and L2) in addition to a non-coding long control region (LCR)[20]. The virus is commonly sexually transmitted and 80 % of all women will have an infection at some point by the age of 45 years[21]. Most infections do not progress into cervical cancer, but virtually all cases of cervical cancer are caused by HPV, and especially by the two high-risk variants HPV-16 and HPV-18. High-risk HPV are associated with higher cancer risk as these encode oncoproteins with a greater ability to interact with regulatory proteins and tumor suppressor genes[18]. The two main oncoproteins are E6 and E7 and causes transformation of the host cell by binding to the tumor suppressor proteins TP53 and RB1, respectively.

Under normal conditions, the cellular level of TP53 is fairly low due to a negative feedback loop causing continuous degradation[22]. However, upon cellular stress such as ionizing radiation causing DNA damage, the degradation is stopped and TP53 works as an activator for transcription of genes needed to induce cell cycle arrest or apoptosis. When a cell is infected with HPV, E6 causes degradation of TP53, and the cell cycle will continue to progress even if the cell is exposed to stress and has severe DNA damage.

The RB1 protein functions as a break on the cell cycle by repressing transcription of genes needed for passage through the G_1 checkpoint, and inactivation of this protein is therefore necessary for the cell cycle progression. Upon HPV infection, E7 targets RB1 and inactivates its function permanently, causing the G_1 checkpoint to be lost.

2.5 MicroRNA

MiRNAs is a group of small non-coding RNAs. The term "non-coding" implies that they are transcribed from DNA, but they are not translated into proteins. Instead, they are involved in post-transcriptional gene regulation by binding to mRNAs resulting in mRNA degradation or translational repression. The regulation is a complex system where one miRNA can have many mRNA targets, and one mRNA can have many miRNA regulators. There are by now 1881 published human precursor miRNA sequences and 2588 mature miRNA sequences (mirbase.org, release 21)[23]. MiRNA nomenclature involves prefix letters annotating the species from which it originates, and to a certain extent, the numbering system is based on the chronological order in which the miRNA was published. For instance, hsa-miR-320 is a human miRNA published after hsa-miR-319.

2.5.1 miRNA biogenesis

MiRNAs are mostly located in intergenic regions, but they are also found within exonic and intronic regions of genes[24]. They are first synthesized in the nucleus as primary miRNA (pri-miRNA) by RNA polymerase II[25], and the pri-miRNA is folded back on itself, forming a hairpin structure (Figure 2.6). These resemble a typical mRNA as they have both 5-cap and poly-A-tail. Next, the hairpin shaped pri-miRNA is transported to the cytosol where an enzyme called DICER cuts out the loop and thereby turns it into double stranded miRNA, consisting of a guide strand and a transient strand. The dicing process is coordinated by a double strand-RNA binding protein called TRBP2. Argonaut protein 2 (AGO2) degrades the transient strand, leaving the single stranded guide miRNA. The length of a processed miRNA is about 20-24 nucleotides. Together DICER, AGO proteins and guide miRNA form a complex called miRNA-induced silencing complex (miRISC) which is acting as a guide to deliver the complex to the target mRNA [26-27].

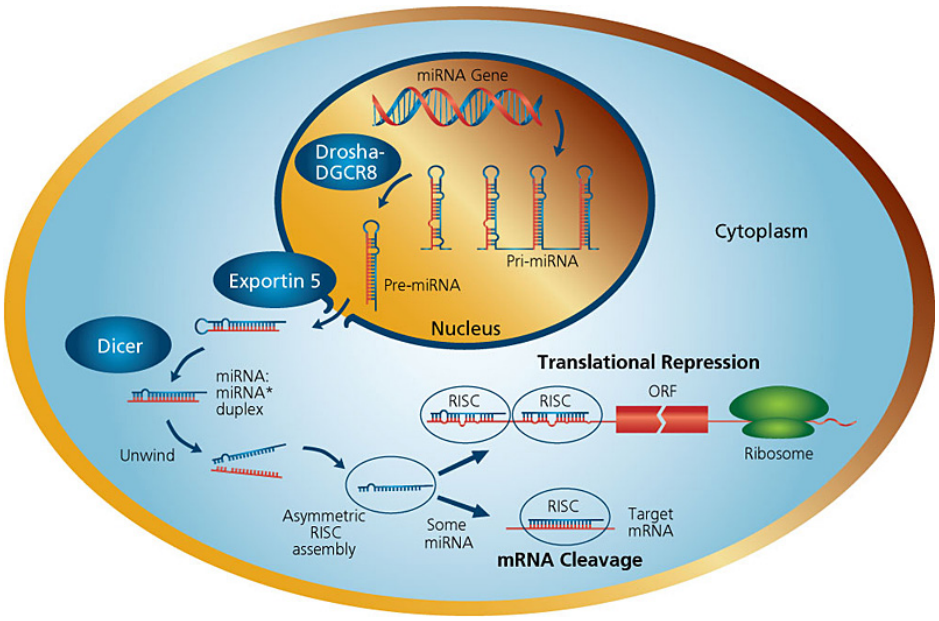

Figure 2.6: miRNA biogenesis and post translational regulation of mRNA. Figure is adapted from Sigma-Aldrich[28].

2.5.2 Gene regulation

Mature miRNAs in complex with DICER and AGO provide post-transcriptional gene regulation by binding to a target mRNA. The method of regulation is a topic of ongoing research, but the general understanding is that the level of complementarity determines the mechanism of regulation. If the miRNA has an imperfect complementarity with the target mRNA, the result is translational repression, while with a perfect or near perfect complementarity, the miRISC complex participates in the degradation of the mRNA[29]. Both processes occur in specific cytoplasmic foci called mRNA processing bodies (P-bodies).

2.5.3 miRNAs in cancer

In normal cells, miRNAs may act as genetic switches or fine-tuners. However, aberrant miRNA expression has frequently been reported in cancer cells and miRNAs are thus suggested to play potential oncogenic or tumor-suppressive roles[30]. Different mechanisms can contribute to deregulation of miRNAs in cancer. MiRNAs can have both oncogenic and tumor suppressive roles, depending on the mRNAs it regulates. A miRNA repressing a tumor suppressor is for instance an oncogenic miRNA, called oncomir, but if the mRNA suppressed encodes an oncogene, the miRNA is a tumor suppressor miRNA. Upregulated miRNAs can be caused by gene amplification or loss of repressive epigenetic markers. Downregulated miRNAs, on the

other hand, can be caused by loss of tumor suppressor transcription factors, repression by oncogenic transcription factors, aberrant DNA hypermethylation, loss of histone acetylation or what is the background for this thesis: genomic loss. Many cellular processes are under influence of miRNA-control[31]. However, the main focus of this thesis is proliferation, cell cycle arrest, apoptosis and survival.

From the discovery of the first miRNA, lin-4, in 1993[32-33], it took eight years before the field really started to expand with the discovery of miRNAs in several different species[34-36] and the understanding of miRNAs in normal physiology as well as pathology emerged. Several works describing miRNA expression profiles have been published, both on cervical cancer and other cancers. By analyzing tumor biopsies from cohorts of patients, the role of different miRNAs has been suggested. For instance in cervical cancer, miR-127 has been found to potentially play a role in lymph node metastasis, and blockage of miR-199a has been shown to cause reduced cell growth[37]. Another study of miRNA in cervical cancer showed that miR-200a might be involved in regulation of metastasis by regulating cell adhesion, and miR-9 is potentially a regulator contributing to altered metabolism of the tumor cells[38].

Mir-320d-1 (hereinafter referred to as miR-320d) is a miRNA located at chromosome 13q where loss was found to correspond with poor outcome from radiotherapy[1]. It belongs to the miR-320 family, which is a family of miRNAs with high sequence similarity, but with different genomic localizations. By now, there are no published studies on miR-320d in cervical cancer. However, findings on miR-320d in other cancers have shown that both up and downregulated levels can contribute to carcinogenesis. Low expression has been found to predict poor outcome of diffuse large B-cell lymphoma[39] and stage II colorectal cancer[40]. Low levels have also been found in serum of women with lymph node-positive breast tumors[41]. Other studies have shown that miR-320d and five other miRNAs have been upregulated in serum from patients suffering from acute myeloid leukemia[42].

2.6 Ionizing Radiation

Radiation can be categorized into ionizing and non-ionizing. The non-ionizing radiation only carries enough energy to excite electrons, meaning that they are moved to a higher energy state. On the other hand, the ionizing radiation has enough energy to free electrons from atoms or molecules, causing what is called ionization[43]. The energy of the radiation depends on the frequency and length of the waves, where high frequency and short wavelengths represent high energy. The radiation dose is given in Gray (Gy), which describes the amount of absorbed radiation. One Gray means that one kilogram of the irradiated matter has absorbed one joule of radiation energy.

2.6.1 Cellular response to radiation

The type of radiation used for cancer therapy is ionizing radiation. When cells are irradiated, the most lethal injury is double-strand breaks of the phosphodiester bonds of the DNA backbone[44]. In order to repair such breaks, the DNA repair machinery is activated. During the repair, the cell cycle is delayed or arrested before further progression. It is the failure of repairing these damages that causes cell death. As cancer cells often divide more rapidly than normal cells and have a diminished DNA repair-system, these are more often vulnerable to radiation[45].

As with many other cancer types, radioresistance is a current problem in cervical cancer therapy. Many different proteins have been found to be involved in DNA repair, but the mechanisms for regulating the repair system is still unclear and remains to be elucidated. Several studies have found miRNAs contributing to the radiosensitivity of tumors and cervical cancer cell lines, such as miR-18a[46], miR-145[47] and miR-218[48], however, none of these are located within the lost region of interest on chromosome 13q.

2.6.2 Radiation therapy

When patients are treated with radiotherapy, the total radiation dose is divided into smaller fractions given on a daily basis. This is to allow the normal healthy cells to repair between each exposure, while the cancer cells to a bigger extent accumulates lethal damages. In treatment of cervical cancer, radiation is typically given in individual doses of 1.8-2 Gy in 25 fractions over 5 weeks, yielding a total dose of approximately 45-50 Gy[49].

2.7 Polymerase chain reaction

The Polymerase Chain Reaction (PCR) is a well-established technique used for amplification of sequences of DNA, but can also be used for measurement of gene expression. In this thesis, cDNA reverse transcribed from miRNA was quantified. PCR is extremely sensitive and very small amounts of target DNA is needed as only one single molecule, in theory, is sufficient for the process to begin.

2.7.1 Basic principles

PCR is based on repetitive amplification of the target cDNA. Needed for this is the target cDNA, oligonucleotide primers, a thermo-stable DNA polymerase, and a supply of nucleotides[50]. Oligonucleotide primers are short sequences of nucleic acids complementary to the 3' end of the cDNA. These are needed for the DNA polymerase to bind to the template and start its enzymatic activity, where the new strand is synthesized from the supply of nucleic acids (Figure 2.7). The method is based on thermal cycling, meaning that the reaction is repeatedly heated and cooled down in order to amplify the cDNA. A classic PCR reaction is started by heating the mixture to the melting temperature, typically around 95 °C. This breaks the hydrogen bonds between the two cDNA-strands, causing them to separate into single-stranded cDNA. Next, the temperature is lowered to the hybridization temperature, the temperature at which the primers anneal to their specific locations at the cDNA, typically around 60°C. At the hybridization temperature, the DNA polymerase will enzymatically elongate the primers by using the supply of nucleotides, called primer extension. The exact temperature is dependent on the DNA-polymerase used in the reaction. Primer extension results in double-stranded DNA, and as every round gives a duplication of each cDNA molecule, the total amount of cDNA will grow exponentially.

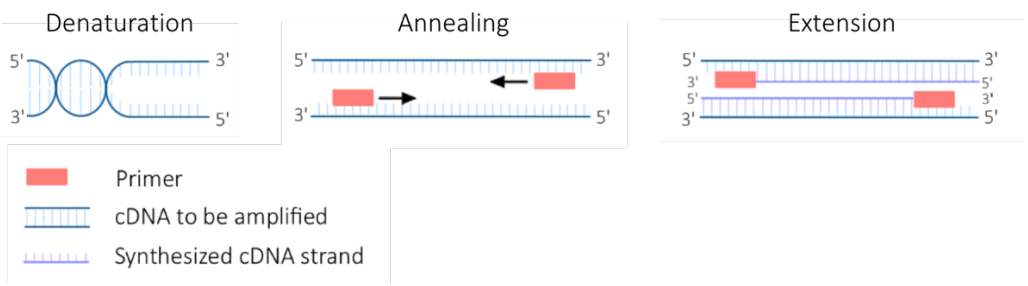

Figure 2.7: Basic principles of one round of PCR. The DNA strand is denatured, primers anneal to the resulting ssDNA and extension of these results in two dsDNA molecules.

2.7.2 Real-time quantitative PCR (RT-qPCR)

Conventional PCR involves many separated steps, such as gel casting, i.e. loading, running and staining the gel, and the computer analysis-step. Also, the quantification of PCR product is based on end point quantification, which is an unreliable measure as the exponential growth of PCR product will eventually cease and reach a plateau.

RT-qPCR is an efficient variant of the PCR technique where amplification and quantitative analysis are done simultaneously, i.e. in real time. In RT-qPCR, the PCR products are fluorescently labeled, resulting in a proportional increase in fluorescent signal as the amount of product increases. The quantitation is based on measurement during the exponential growth in the repeated reactions. The amount of cDNA in a sample is given as a Ct (cycle threshold) value, which is defined as the number of cycles needed for the fluorescent signal to exceed a given threshold value[51] (Figure 2.8). One difference in Ct value represents a doubling of the amount of cDNA, i.e. a sample with Ct value 22 has twice as much cDNA as a sample with Ct value 23.

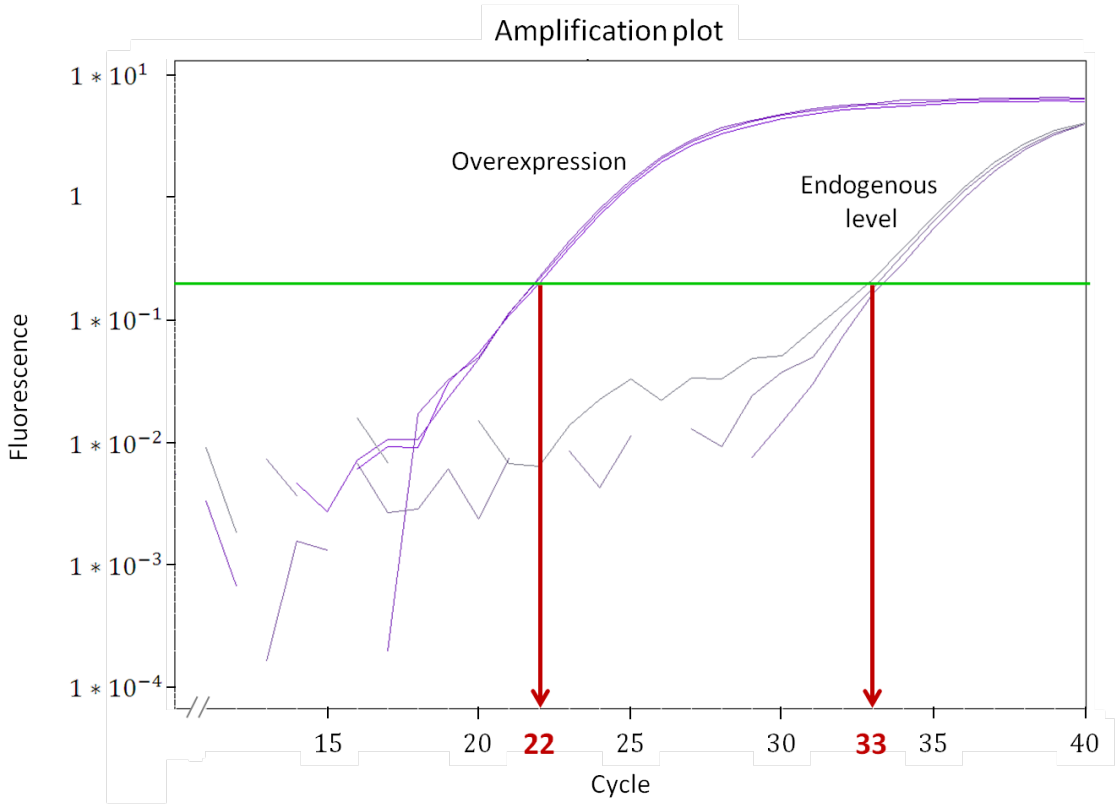

Figure 2.8: Amplification plot showing the Ct-values resulting from samples with overexpressed miRNA (Ct: ~22) and endogenous levels (Ct: ~33). The green line represents the threshold for the fluorescent signals and is set to 0.20.

2.7.3 $2^{-\Delta\Delta Ct}$ method

The Ct values can be used for relative quantification of expression level for the gene of interest. Different methods can be used, but only the Livak method[51-52], also known as the $2^{-\Delta\Delta Ct}$ method, will be presented for here, exemplified by miRNA overexpression (Formula 2.1). A sample is treated to overexpress a specific miRNA, and the expression is calculated relative to a reference gene that is stable both in the sample with overexpression and in the negative control. The method is based on the assumption that the amplification efficiency for both the gene of interest and the reference gene is close to 100% and within 5 % of each other (see more details in section 3.5.1). However, RT-qPCR assays with amplification efficiencies between 90 and 110 % can be used[53].

First, the Ct of the gene of interest is normalized to that of the reference gene for both the treated sample and the negative control sample.

Formula 2.1: Steps of the $2^{-\Delta\Delta Ct}$ method

a) $$\Delta Ct\ (treated\ sample) = Ct_{gene\ of\ interest,\ \ treated} - Ct_{reference\ gene,\ \ treated}$$

$$\Delta Ct\ (negative\ control) = Ct_{gene\ of\ interest,\ \ neg.cont.} - Ct_{reference\ gene,\ \ neg.cont.}$$

Next, the ΔΔCt is calculated to find the difference between ΔCt of the treated sample and ΔCt of the negative control.

b) $$\Delta\Delta Ct = \Delta Ct_{(treated\ sample)} - \Delta Ct_{(negative\ control)}$$

Finally, the normalized expression ratio is calculated by using the following formula:

c) $$Normalized\ expression\ ratio = 2^{-\Delta\Delta Ct}$$

The number obtained from this equation is the fold increase or decrease of the gene of interest in the treated sample relative to the negative control, and normalized to the expression of the reference gene.

2.7.4 Locked nucleic acid (LNA)

Detecting miRNA can be challenging due to their short length and their high sequence similarity between closely related miRNAs. Normal nucleotides within a DNA-strand switch between S- and N- conformation, where the N-conformation is the most stable and also the conformation that is optimal for binding to complementary RNA. In the case of miRNAs, these switches result in an inaccurate binding due to the short length of the strand. To prevent this problem, modified nucleotides called locked nucleic acids (LNAs) are incorporated in the RT-qPCR primers[54]. The LNAs have a methylene bridge between 2' O and 4' C, locking them into the ideal N-conformation. This enhances the binding affinity of the primer by preorganizing the conformation of the nucleotides (Figure 2.9).

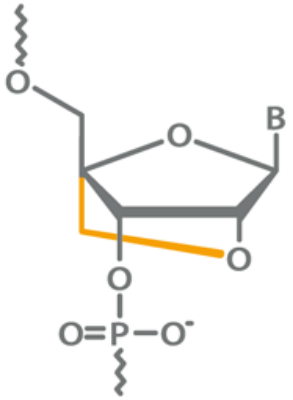

Figure 2.9: The structure of LNA. The orange line between 2'O and 4'C is the methylene bridge locking the nucleotide into the N-confirmation. Figure adapted from Exiqon[54].

The increased stability of the LNA-RNA duplex also improves the ability for distinguishing perfect matches from single mismatches. The melting temperature for a perfect match with a standard DNA-based primer can for instance be 35°C, while one mismatch incorporated decreases the melting temperature to 25°C. For the corresponding duplex of RNA and LNA, the perfect match has a melting temperature at 71°C while one mismatch results in a melting temperature at 45°C (Figure 2.10). The large difference in melting temperature between mismatch and perfect match for LNA primers makes it easier to find the hybridization temperature where only the perfect match is detected. This makes the results much more reliable.

The specificity and sensitivity of the oligonucleotide primer can be optimized by varying the LNA content. The same length of an oligonucleotide can have a higher melting temperature by increasing the LNA content, and oligonucleotide sequences of different length can have the same melting temperature by adjusting the DNA-LNA ratio.

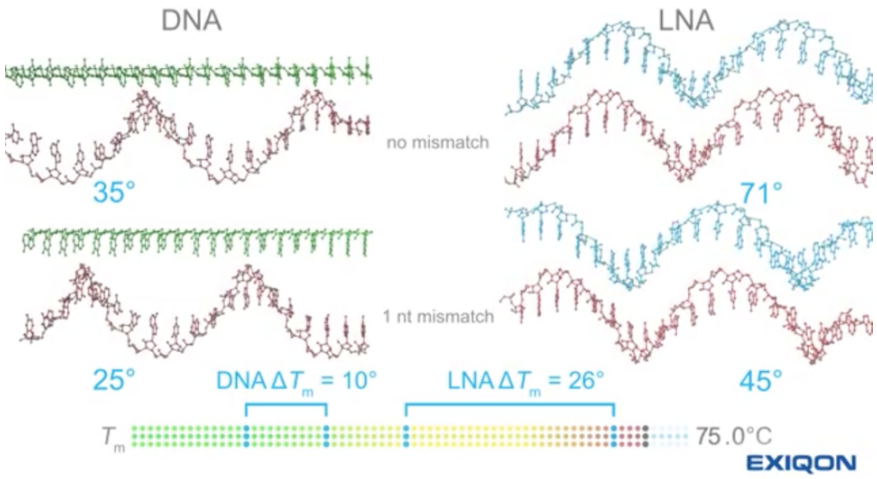

Figure 2.10: Incorporation of LNAs increases the difference in melting temperature for perfect matches and mismatches between the miRNA and the primer. With a normal primer, the difference in melting temperature between perfect match (35°C) and one mismatch (25°C) is 10°C. By using LNAs, the difference can be increased to 26°C (perfect match: 71°C, one mismatch: 45°C). Figure is adapted from instruction video from Exiqon[55].

2.7.5 Incorporation of fluorescent signal

The increase in PCR product is measured as increase in fluorescent signal. One method is primer-based assays, such as TaqMan, where primers specific for the genes of interest are used. The TaqMan primer has a fluorescent reporter dye attached to the 5'-end and a quencher attached to the 3'-end. Fluorescence from the reporter is quenched when the primer is intact. When the DNA polymerase extend the PCR product during the amplification cycles, the reporter and quencher is cleaved apart from each other, and the reporter dye will emit its fluorescence. Another option for fluorescent signaling is SYBR® Green, which is the dye we used in our experiments. This dye is non-sequence specific and fluoresces when bound to dsDNA in general (Figure 2.11). No primers specific for the dye are required, but it may generate false positive signals unless highly specific primers for the RT-qPCR are used. The need for specific primers is therefore crucial to yield correct information about the gene of interest.

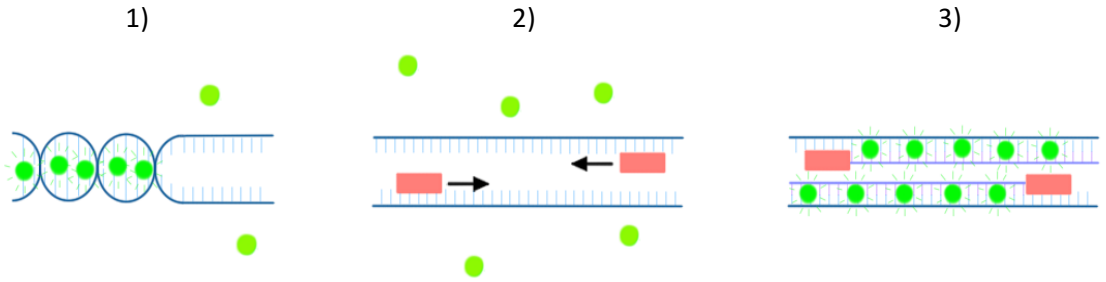

Figure 2.11: 1) SYBR® Green fluoresces when bound to double stranded cDNA 2) When the cDNA is denatured, the SYBR® Green is released, the fluorescence is drastically reduced 3) Amplification of the cDNA results in a net increase in fluorescence as the amount of double stranded cDNA is increasing.

2.7.6 Melting curve analysis

When non-specific fluorescent dyes such as SYBR Green® are used, an additional melting curve analysis should be performed to control for unspecific PCR products and primer-dimers, even though the primers used are supposed to be highly specific[56]. The melting curve analysis is programmed to be performed when the amplification is completed. The temperature is gradually increased from 60 ºC to 95 ºC, causing the double stranded cDNA to melt into single stranded cDNA and the fluorescent dye will dissociate. By monitoring the decrease in fluorescence, the exact melting temperature for the PCR product is measured and shown as a

melting curve (Figure 2.12). Presence of non-specific products can be seen as additional peaks next to the peak representing the amplified product.

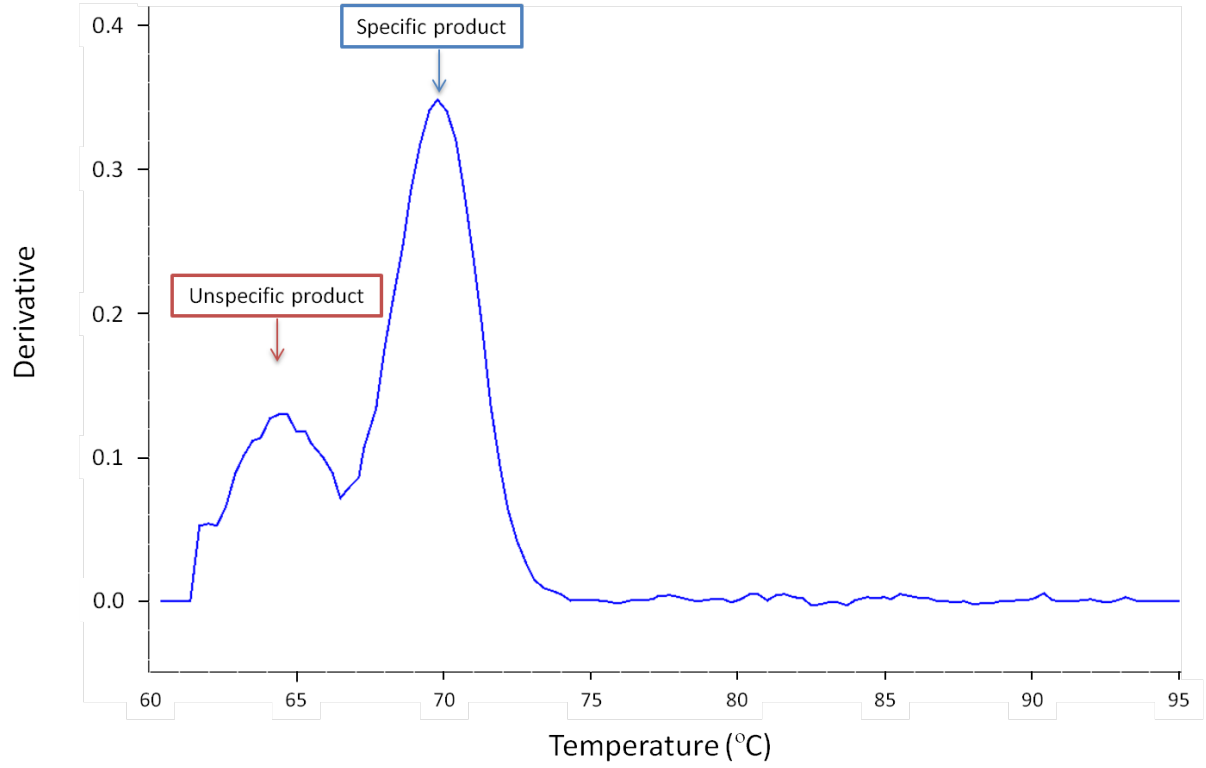

Figure 2.12: Melting curve analysis showing the melting temperature of the PCR product of interest around 70 °C and of an additional unspecific product around 65 ºC. The derivative values on the y-axis represent change in fluorescence.

2.7.7 RNA Spike-ins

RNA spike-ins are synthetic control templates added prior to the cDNA synthesis reaction. These provide controls for the RNA isolation, the cDNA synthesis and the RT-qPCR[57-58]. During the RNA isolation steps, compounds might be included that can inhibit the cDNA synthesis or the RT-qPCR. Such inhibition will cause altered efficiencies for these reactions, and will eventually cause erroneous Ct-values. To control for such errors, equal amounts of spike-in template are added to each reaction. The spike-in templates are amplified in the RT-qPCR by adding spike-in-specific primers, and if everything is in order, the Ct-values for all spike-in reactions are expected to be the same. Additional controls should include cDNA synthesis reactions without template or enzyme, to control for contaminations and for genomic DNA, respectively.

2.8 Transfection

Transfection is the name given to the process where nucleic acids are introduced into eukaryotic cells by nonviral methods[59]. This can be done to study overexpression or downregulation of a gene or a miRNA. Cells can be transfected on a permanent basis, called stable transfection, or on a transient basis, called transient transfection. With transient transfection, the introduced nucleic acids will gradually be lost by cell division and degradation, unlike the stable transfection where the nucleic acids often are incorporated in the cell genome, causing long-term overexpression or inhibition. As the nucleic acids are hydrophilic, the delivery over the hydrophobic cell membrane is a challenge. Various chemical-, lipid- and physical methods can be used to overcome this.

In the following experiments, lipid-based transfection was used. The reagent consist of lipids with positively charged head-groups[59], which associate with the negatively charged phosphates on the nucleic acids, and thereby form a DNA-lipid complex. This complex can enter the cell, either by endocytosis, or by fusion with the plasma membrane.

2.8.1 miRNA mimics

miRNA mimics are short double-stranded RNAs intended to mimic the function of native miRNA (Figure 2.13). They are chemically modified in such a way that the guide strand is the strand preferred over the transient strand for binding with miRISC[60]. The purpose of transfecting cells with mimics is to upregulate the level of a specific miRNA. Transfection with a negative control is used to control for phenotypic changes caused by the transfection itself rather than the specific miRNA of interest. This involves transfection with a miRNA from *C. elegans* which has minimal sequence identity with any miRNA in human. Additionally, a negative control called mock is performed with transfection reagents only. This is to control for phenotypic changes caused by the transfection reagents.

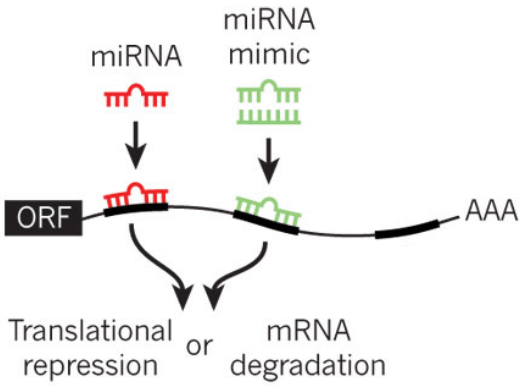

Figure 2.13: Double stranded miRNA mimic, mimicking the function of native miRNA. Figure adapted from E.M. Small and E.N. Olson[61]

2.9 Flow cytometry

2.9.1 The flow cytometer

A flow cytometer measures and analyses multiple characteristics of cells or other particles in solution, usually within the range of 0.2-150 µm in diameter[62]. Parameters to be measured are relative size, relative inner complexity and relative fluorescence intensity. Fluorescent labeling can be used to look for more distinct features of the cell, such as apoptosis and cell cycle distribution, depending on the fluorochrome used. Fluorescence is based on the principle that when a fluorochrome is illuminated with the proper wavelength, the compound will be excited and emission of light of a higher wavelength will follow, which is the signal detected by the flow cytometer. The flow cytometer consists of three subsystems: the fluidic system, the optical system and the electronic system.

The fluidic system is where the sample enters the instrument, and the fluidics brings the cells in the sample to the interrogation point, which is where they interact with the excitation source for analysis (Figure 2.14). The functions of the optical system are excitation of the sample and signal collection. The electronic system converts the light signals into numerical data and removes weak signals caused by cell debris and electronic noise.

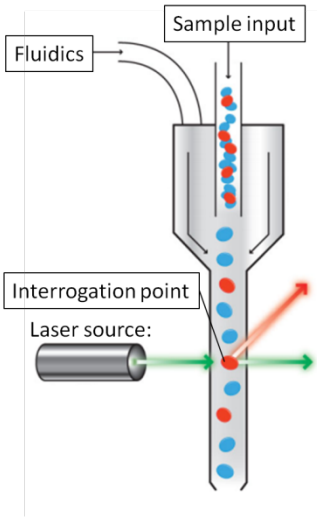

Figure 2.14: Simplified schematic overview of the fluidic system of a flow cytometer. Figure adapted from Faculty of Medicine and Dentistry, University of Alberta[63] (modified).

2.9.2 TUNEL assay

Terminal deoxynucleotidyl transferase dUTP nick end labeling (TUNEL) is a method that can be used for detecting apoptotic cells. When cells undergo apoptosis, the DNA is cleaved into blunt-ended fragments of typically 180-200 bp[64-65]. These fragments are identified by the terminal deoxynucleotidyl transferase (TdT), which is an enzyme catalyzing the addition of dUTP to the 3'-hydroxyl nicks. The dUTP used in this thesis is biotinylated, which provide indirect detection by binding to Cy5-labeled streptavidin (Figure 2.15). Cy5 is a dye excited by red light around 650 nm and emitting around 670 nm[66]. Other deoxynucleotides than dUTP can also be used in different variants of TUNEL assays. The DNA labeling makes it possible to analyze the percentage of apoptotic cells in the flow cytometer.

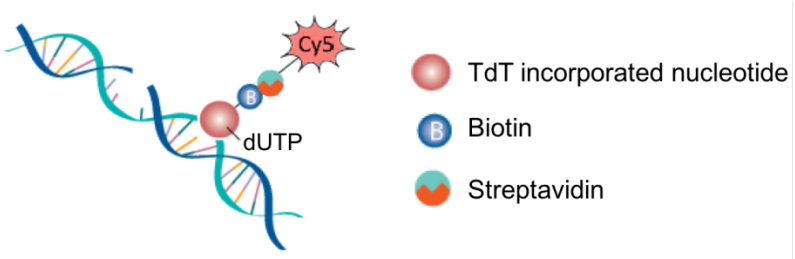

Figure 2.15: TUNEL assay involving Cy5-labeling of apoptotic DNA. Modified version of figure found on the webpages of R&D systems[66]

2.9.3 Cell cycle distribution

The cell cycle distribution can be determined by measurement of the DNA content of each cell in a cell population. Hoechst 33258 is frequently used for this purpose as it binds to the minor groove of dsDNA, and can thereby give information about where in the cell cycle every cell is. It is a blue fluorescent dye excited by ultra violet light around 352 nm and emitting around 461 nm[67]. In the G_1 phase, most cells have the same DNA content, and these are seen as the first peak of a DNA histogram showing cell cycle distribution (Figure 2.16). During S phase, the DNA is continuously replicated, meaning that the cells within this phase have various amounts of DNA, which can be seen as the long distribution covering various amounts of fluorescence from Hoechst 33258. In the G_2/M phase, the DNA is fully replicated and the cells have twice as much DNA as in the G_1 phase. As these cells have the same amount of DNA, they are seen as a peak rather than a longer distribution.

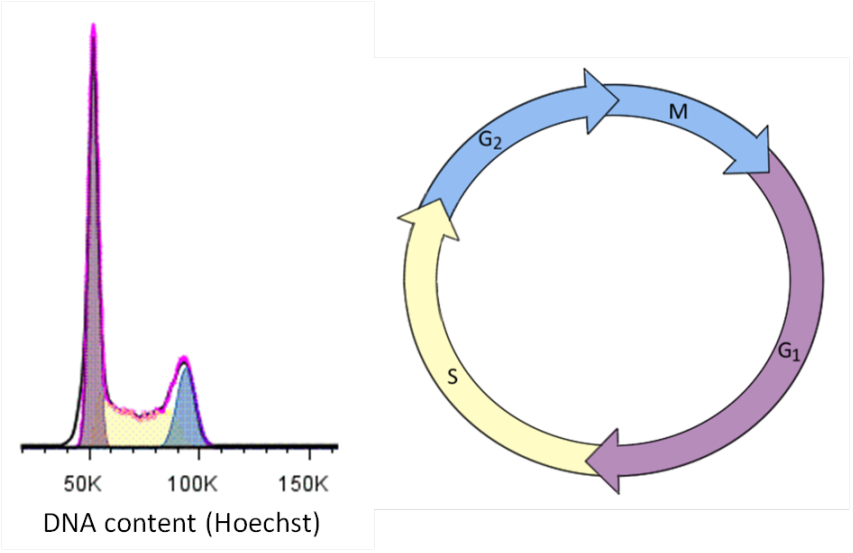

Figure 2.16: Cell cycle distribution shown as a DNA histogram and colored in relation to the cell cycle. G_1 cells are colored in purple and have half the amount of DNA as G_2/M cells (blue). S phase cells have various amount of DNA and are shown in yellow. The analysis is performed on a flow cytometer.

3 Methods

Schematic overview of the study design is shown in Figure 3.1. Methodological parts include establishment of RT-qPCR for analyzing miR-320d expression before and after upregulation with miRNA mimics. Biological parts include measurement of apoptosis, cell cycle distribution, survival and radiosensitivity. All reagents, equipment, instruments and software used can be found in Appendix 17.

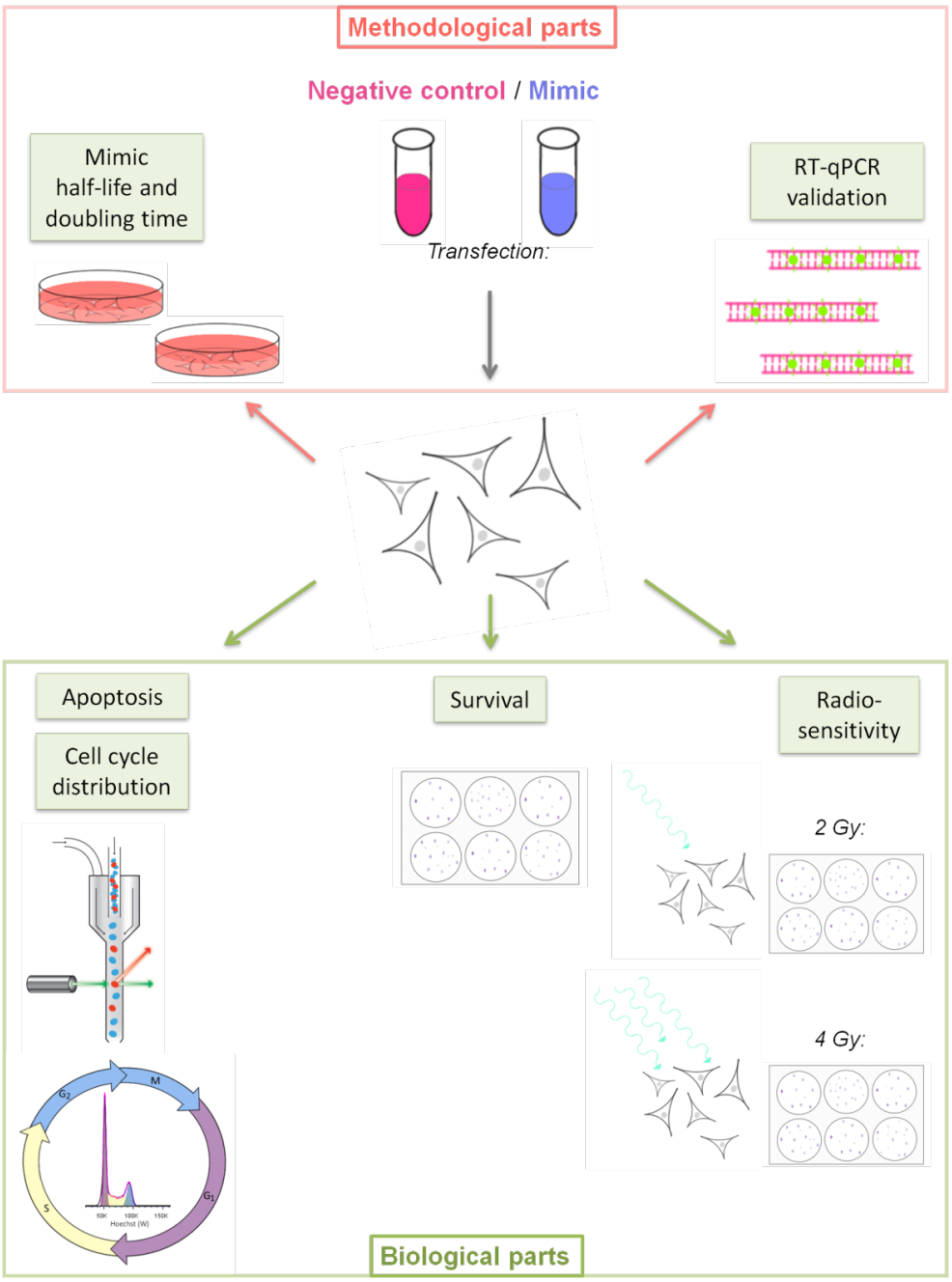

Figure 3.1: Schematic overview of the study design

3.1 Cell lines

The cell lines HeLa and SiHa used in the experiments are both immortalized epithelial cell lines obtained from human cervical tumors. These cell lines are useful for research as they both origin from the two most common types of cervical cancer and are infected with high-risk HPV. HeLa cells are HPV-18 infected adenocarcinoma cells, and SiHa cells are HPV-16 infected cells obtained from squamous cell carcinoma[68-69]. In addition, sequencing data of miRNA expression were available in our group for both cell lines, and were useful for selection of miRNA to be studied in this thesis.

HeLa and SiHa are both adherent cell lines growing as monolayers in culture. The cells were cultured as described in Appendix1 with Dulbecco's Modified Eagles Medium with 10 % Fetal Bovine Serum (FBS), 1 % Penicillin Streptomycin and 1 % L-glutamine added. Cells used for experiments were seeded in 6-well plates, each well with a surface area of 9.62 cm^2.

3.2 Selection of miRNA

Sixteen miRNAs are located within the lost 13q-region (13q13.1-q21.1), which was found to be associated with poor prognosis in cervical cancer patients in previous work[1] (Figure 3.2). To select a suitable miRNA for further studies, two criteria were used. First, the miRNA should be expressed in the cervical cancer cell lines HeLa and SiHa, since this is necessary for looking at both up- and downregulation of the miRNA. Second, there should be a considerable variation in expression of the selected miRNA between the 90 cervical patients for which we had available data. A miRNA with a large variation is more likely to be of clinical relevance for the aggressiveness of the cancer, as some patients have a 13q loss while others do not. MiR-320d fulfilled these criteria and was selected for further studies.

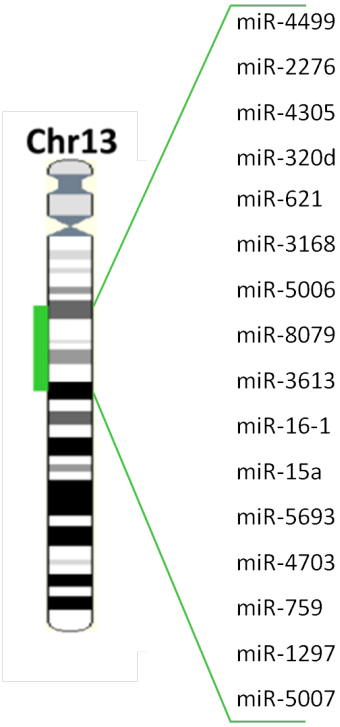

Figure 3.2: The sixteen miRNAs located at the lost region of chromosome 13q (13q13.1-q21.1). Figure adapted from Lando et al.[1] (modified).

Reference gene

To remove technical and biological variations not related to the effect of overexpressing miR-320d, a reference gene was needed for normalization. The best reference gene to use when working with miRNAs is another miRNA of approximately the same size, that has the same extraction efficiency and stability and which is expressed within the same range as the miRNA to be studied. MiR-103a-3p was expressed in both cell lines, and was selected based on these criteria and recommendations from Exiqon.

3.3 RNA isolation

RNA isolation was carried out according to the protocol in Appendix 2. The miRNeasy Mini Kit was used for isolation of total RNA consisting of 18 nucleotides or more[70], thereby including miRNAs. The reagent used for cell lysis, called QIAzol Lysis Reagent, inhibits RNases in addition to removing most of the cellular DNA and proteins from the lysate. Addition of chloroform followed by centrifugation was performed to separate the homogenate into aqueous and organic phases. RNA settled in the aqueous phase, and this phase had ethanol added to provide appropriate binding conditions to the membrane of the RNeasy Mini spin column included in the kit. The RNA was extracted from the sample by binding to the membrane, while phenol and other contaminants were washed out by centrifugation. Elution of the RNA was done by adding nuclease free water to the membrane. The concentration of RNA was measured on a NanoDrop 2000 Spectrophotometer before storage at -80°C.

3.4 cDNA synthesis

In order to quantify the levels of miRNA, first-strand cDNA had to be made and further used as template for RT-qPCR analysis. The synthesis was carried out according to the protocol found in Appendix 3 using the GeneAmp® PCR System 9700. During the first-strand cDNA synthesis, a poly-A tail was added to the mature miRNA template. A reverse transcriptase enzyme synthesized the cDNA by elongation of a poly-T primer with a 3' degenerate anchor and 5' universal tag (Figure 3.3). The sample was incubated at 42°C for 60 min, allowing the cDNA synthesis to occur, followed by a 95°C heat-inactivation of the enzyme for 5 min.

Figure 3.3: cDNA synthesis. A) Addition of poly-A tail to mature miRNA template. B) cDNA synthesis by elongation of poly-T primer. Figure adapted from instruction manual provided by Exiqon[58].

3.5 RT-qPCR

The RT-qPCR analysis was carried out according to the protocol in Appendix 4. Master mixes containing the desired LNA primers were placed in wells of a MicroAmp® Fast Optical 96-well PCR plate. cDNA resulting from all three transfection treatments, including the controls without template or enzyme, were added. Triplicates of all cDNA-templates were analyzed, in addition to duplicates of non-enzyme controls and the non-template control. Spike-in controls were tested for all cDNA samples. Applied Biosystems 7900HT Fast Real-Time PCR system was used for the amplification and melting curve analysis. The software SDS 2.3 was used for setting up the content of each well and for analyzing the results.

3.5.1 PCR efficiency

A robust RT-qPCR assay is recognized by displaying a linear standard curve (R^2 >0.980), high PCR efficiency (90-110%) and consistency across replicate reactions[52-53]. The standard curve was generated by making serial dilutions for each cDNA sample and the log of the dilution was plotted against the mean C_T value obtained from the amplification cycles. PCR efficiency, also called amplification efficiency, is a measure of the amount of PCR product amplified. Ideally, each round of amplification should result in complete doubling of PCR products, corresponding to a 2-fold increase or a reaction efficiency of 2. The PCR efficiency was calculated from the slope of the standard curve and used in Formula 3.1. Efficiencies close to 100 % corresponds to high quality and a reproducible assay.

Formula 3.1: Calculation of PCR efficiency

$$\% \, PCR \, efficiency = \left(10^{\frac{1}{slope}} - 1\right) * 100$$

3.6 Transfection

Transfection was performed to introduce the miR-320d mimic and the negative control into the cells. The negative control was used to control for phenotypic changes caused by the transfection itself rather than the miR-320d mimic. This involved transfection with a miRNA from *C. elegans* which has minimal sequence identity with any miRNA in human. Additionally, a negative control called "mock" was included, where only the transfection reagent was applied. This was to control for phenotypic changes caused by the transfection reagent itself.

The experiment was carried out according to the transfection protocol in Appendix 5. Cells were seeded out in 35 mm^2 dishes one day before the transfection, approximately 300 000 HeLa cells and 625 000 SiHa cells. A lipid-based transfection reagent was used for transfecting the negative control miRNA (5 µM) and miR-320d mimic (5 µM) into the cells. Harvesting was done 22 hours post-transfection. Workflow is shown in Figure 3.4.

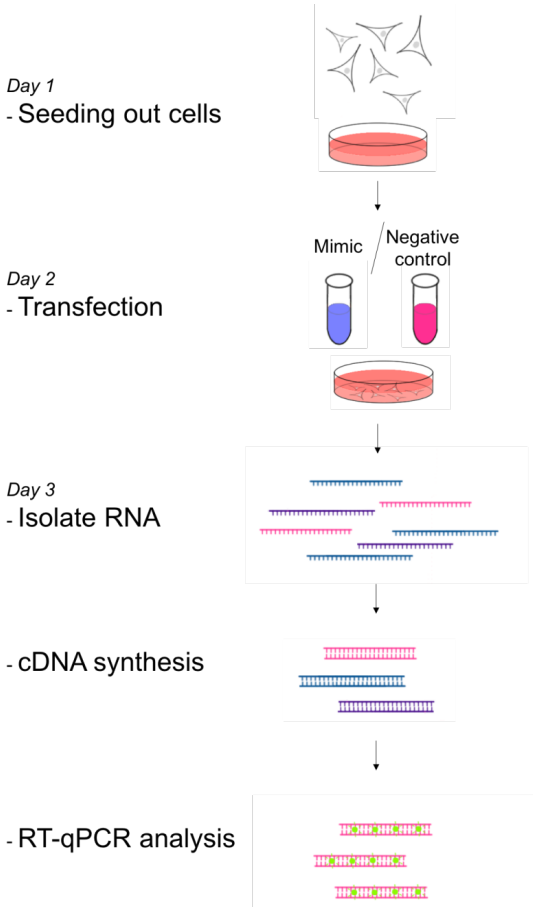

Figure 3.4: Workflow for transfection of SiHa and HeLa cells, from seeding out cells to analyze miRNA expression on RT-qPCR

3.6.1 Transfection half-life

The cells were transiently transfected, meaning that the introduced nucleotides only exist in the cells for a limited time. To examine for how long miR-320d was upregulated, cells were transfected and then seeded out in 10 (HeLa) or 12 (SiHa) 35mm^2 dishes with complete culture medium the third day. 5000 cells were seeded into each dish. RNA was isolated from one dish every day over a period of 10-12 days and the miRNA levels were examined by using RT-qPCR. The log transformed fold induction was calculated from the Ct-values and plotted as a function of time (days). A regression line was fitted to the data, describing an exponential relationship between fold induction and time according to Formula 3.2, where t is time, α is the initial relative upregulation at time t_1 (day 1) and c is the constant of decay. The constant c was further used to calculate the half-life ($t_{1/2}$) for the mimic decay by using Formula 3.3.

Formula 3.2: Function for exponential decay of miRNA mimics upregulation

$$F_{fold\ induction}(t) = \alpha\, e^{-ct}$$

Formula 3.3: Half-life of miRNA mimics

$$t_{1/2} = \frac{\ln(2)}{-c}$$

3.7 Proliferation (cellular doubling time)

The proliferation experiment (Appendix 6) was performed to calculate the doubling time of cells transfected with miR-320d and the negative control cells, and to compare these numbers with the transfection half-life.

50 000 cells were plated out in T_{25} cell culture flasks. The number of cells in three flasks was determined every day using a coulter counter (Beckman counter Z2). Figure 3.5 shows the daily procedure for cell counting.

The cell numbers obtained were used for plotting a growth curve, which made it possible to determine the doubling time (T_d) for each cell line and treatment. T_d is the time it takes for the cells to complete one cell cycle and divide, and can be calculated from the exponential growth phase using Formula 3.4, where N_0 and N_t are the initial and final number of cells within the exponential phase, and t is the time in hours.

Formula 3.4: Cell doubling time

$$T_d = \frac{\ln(2)}{\left(\frac{\ln\left(\frac{N_t}{N_0}\right)}{t}\right)}$$

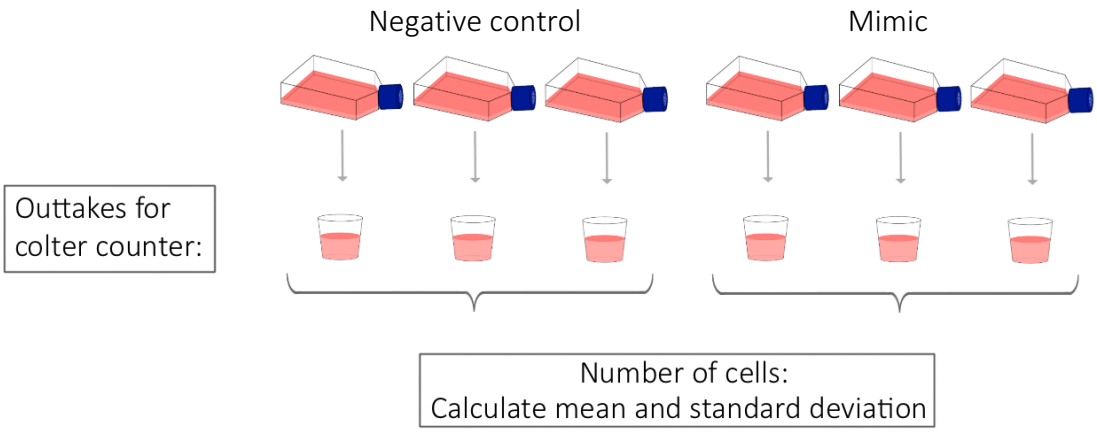

Figure 3.5: Illustration of the daily procedure for counting cells in the proliferation assay. The same procedure was performed for mimic and negative control.

3.8 Clonogenic assay and radiosensitivity

When cells are cultured, not all will survive, and especially treatments such as transfection and radiation will affect cell survival. Clonogenic assay is a technique used to determine the average survival of cells within a population by measuring the cells ability to divide and form colonies (clonogenicity). A colony will have to contain at least 50 cells to be valid[71]. Clonogenic assay was performed to determine cell survival and radiosensitivity, which is the susceptibility a cell has for the damaging effect of ionizing radiation. Radiosensitivity can be illustrated in a dose response curve where the relationship between radiation dose and survival fraction is shown. Survival fraction is the proportion of cells surviving the radiation. The cells were irradiated with an X-ray generator (Faxitron CP160, 160 kV, 6.3 mA) at a dose-rate of 1 Gy/min.

The experiment was carried out as described in Appendix 7. Three parallels of a predetermined number of irradiated cells (Table 3.1) were seeded out and left in the incubator for 13 (HeLa) or 16 (SiHa) days (Figure 3.6). The resulting colonies were fixed and stained as described in Appendix 8. Colonies consisting of 50 cells or more were counted under a light microscope. Plating efficiency (PE) is defined as the percentage of cells that grows into colonies, and was calculated from Formula 3.5. Survival fraction was calculated from Formula 3.6.

Formula 3.5: Plating efficiency

$$PE = \frac{Number\ of\ colonies\ counted}{Number\ of\ cells\ plated} * 100$$

Formula 3.6: Survival fraction

$$SF = \frac{\frac{Number\ of\ colonies\ counted}{Number\ of\ cells\ plated}}{PE_{0\ Gy\ cells}}$$

Table 3.1: Number of cells plated for study of radiosensitivity

	Radiation dose (Gy)		
SiHa/HeLa	0	2	4
Number of cells plated	300	1 000	10 000

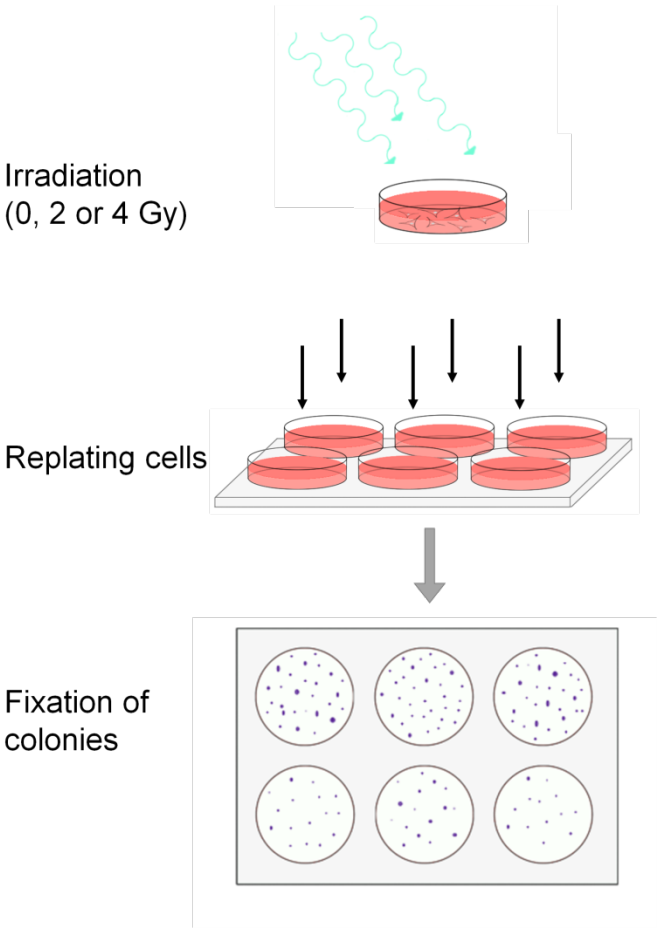

Figure 3.6: Workflow for plating out cells for clonogenic assay in order to determine average cell survival within the population, and to determine radiosensitivity.

3.9 Flow cytometry analysis

The cells transfected with miR-320d mimic and with negative control were harvested and frozen according to Appendix 9 and further prepared for TUNEL assay to look for apoptosis and stained with Hoechst to study cell cycle distribution (Appendix 10). For the TUNEL assay, apoptotic Reh cells (acute lymphoblastic leukemia cells irradiated with 4 Gy) were used as positive control. The cell cycle distribution was analyzed to look for accumulation of cells in a specific cell cycle phase as a cause of the transfection with miR-320d. Three parallels of experiments were run, and when no differences in cell cycle distribution or apoptosis were detected 22 hours post-transfection in the two first experiments, the third experiment was analyzed 46 hours post-transfection.

Methanol was used for fixating cells and preserving their cell cycle phase. Due to different emission spectra for Hoechst and Cy5, cell cycle distribution and fraction of apoptotic cells was measured simultaneously (Figure 3.7). A BD LSR II Flow cytometer was used for running the samples and the software package FlowJo (version 7.6.5) was used for analyzing all flow cytometry data.

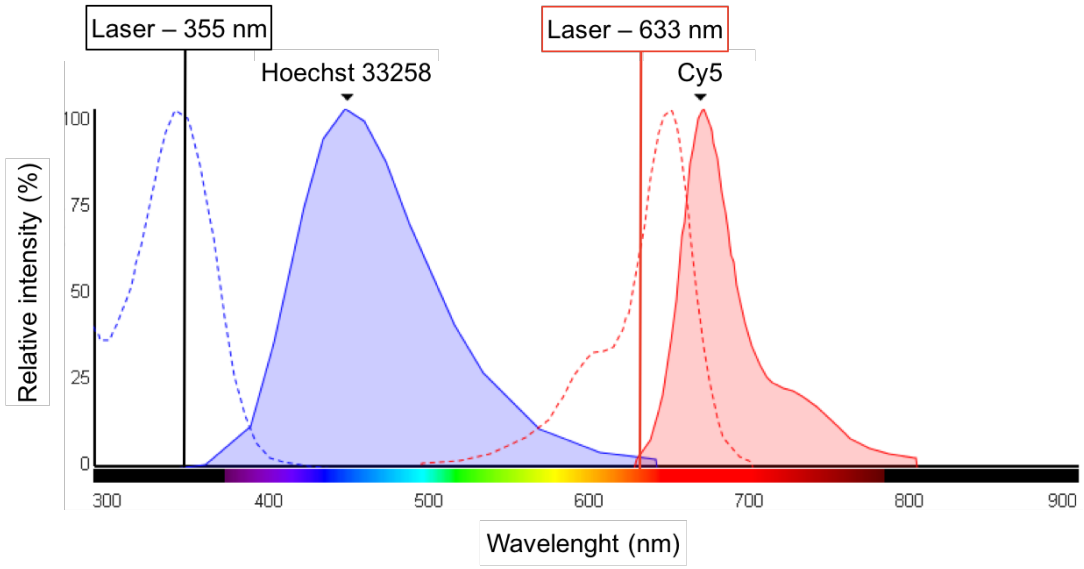

Figure 3.7: Excitation and emission spectra for Hoechst 33258 (blue) and Cy5 (red). Excitation spectra are marked with dotted lines and emission spectra with solid lines. Hoechst 33258 is excited at ~352 nm and emits at ~461 nm[67]. Cy5 is excited at ~650 nm and emits at ~670 nm[66]. The BD LSR II Flow cytometer was used with UV laser (355 nm) for exciting Hoechst and red laser (633 nm) for exciting Cy5. Figure is adapted from ThermoFisher Scientific[72].

When using flow cytometry, a signal may originate from two cells clustered together (doublets), especially when the cells are adherent. To reduce this problem, the cells were filtered and gently vortexed before analysis. However, post-processing of the data was still needed to collect information about single cells only. By combining the width and area of the recoded pulses, the single cells were selected for analysis by drawing them into a gate (Figure 3.8).

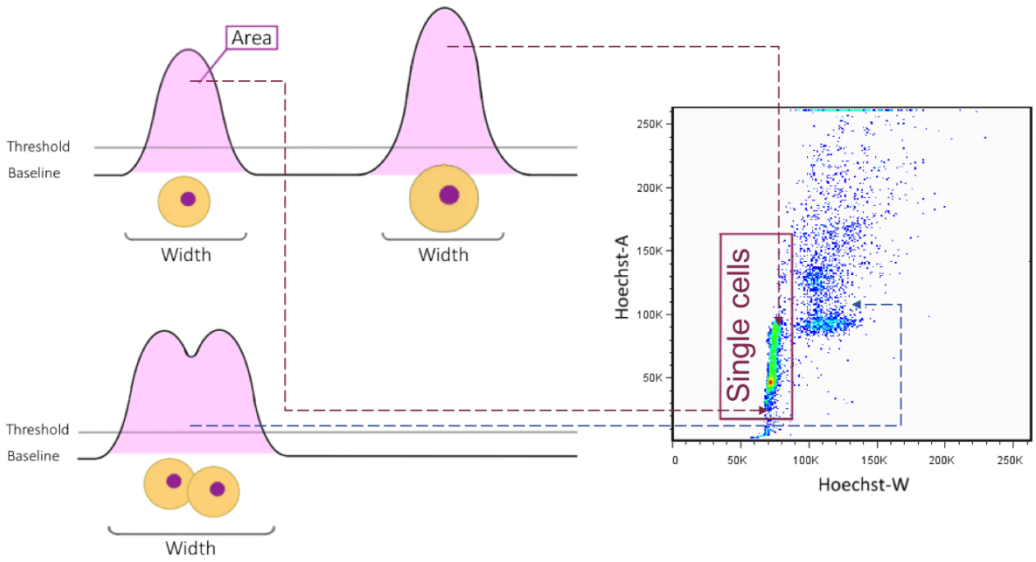

Figure 3.8: Separation of single cells from doublets. When a cell passes the laser beam of the flow cytometer, it gives rise to an electrical pulse, shown in the diagram as a dot. With width on the x-axis, narrow peaks are separated from wider peaks. Single cells give rise to approximately the same width, while doublets are much wider as the peaks from the two cells are merged together. Hence, single cells are located to the left in the plot and can be separated from the doublets by drawing a gate around them.

3.10 Statistical analysis

Standard deviation (SD) was used throughout this thesis to describe the typical difference between the data points and their mean value. In order to determine statistical significance of differences seen in the experiments, Student's t-test with two-tailed distribution was used as the datasets resulting from the experiments were considered to follow normal distribution. Regression was performed using Microsoft Excel 2007.

4 Results

4.1 Selection of miRNA

Of the 16 miRNAs located at 13q13.1-q21.1, only three miRNAs were expressed in HeLa and SiHa cells (Table 4.1). These were also the only miRNAs that were expressed in patients, where miR-320d had the largest variation in expression between the samples. MiR-15a is an early discovered and well-studied miRNA. As the nomenclature give an indication of, miR-3613 was discovered later, and is barely studied at all. Even though it is expressed in both HeLa and SiHa cells, RT-qPCR showed endogenous levels too low for further studies (results not shown). MiR-320d on the other hand, is slightly more studied, but with no publications on cervical cancer. RT-qPCR analysis showed endogenous expression levels giving Ct-values of 30-31, which was suitable for further studies of overexpression.

Table 4.1: Location, expression in cell lines and expression/range in patients for the 16 miRNAs located at 13q13.1-q21, in which loss has been found to correspond with poor prognosis for cervical cancer patients after radiotherapy.

miRNA	Locus (Mb)	Expressed in HeLa & SiHa cells	Expressed in patients	Range in patients
miR-4499	20.4	-	-	-
miR-2276	24.2	-	-	-
miR-4305	39.7	-	-	-
miR-320d	**40.7**	**Yes**	**Yes**	**0.58-4.28**
miR-621	40.8	-	-	-
miR-3168	41.1	-	-	-
miR-5006	41.6	-	-	-
miR-8079	44.2	-	-	-
miR-3613	50.0	Yes	Yes	4.57-6.52
miR-16-1	50.0	-	-	-
miR-15a	50.0	Yes	Yes	8.30-9.83
miR-5693	51.3	-	-	-
miR-4703	51.6	-	-	-
miR-759	52.8	-	-	-
miR-1297	54.3	-	-	-
miR-5007	55.2	-	-	-

4.2 Establishment of method for analyzing miR-320d expression with RT-qPCR

4.2.1 PCR Efficiency

PCR efficiency was calculated to confirm a sufficient robustness and reproducibility of the RT-qPCR assay. Serial dilutions of cDNA from untreated HeLa cells were analyzed and used for generation of standard curves (Figure 4.1). Linear regression showed that cDNA dilutions between 80x and 5120x were within the linear range of the dilution curve for both miR-320d ($R^2 = 0.996$) and the reference gene, miR-103a-3p ($R^2 = 0.989$). In the linear range, increasing cDNA dilutions resulted in corresponding increase in Ct values and the equations for the fitted curves were used to calculate PCR efficiencies of 110 % for miR-320d, and 107 % for the reference gene miR-103a-3p. 320x dilutions were chosen for the further experiments as these involved upregulation of miR-320d.

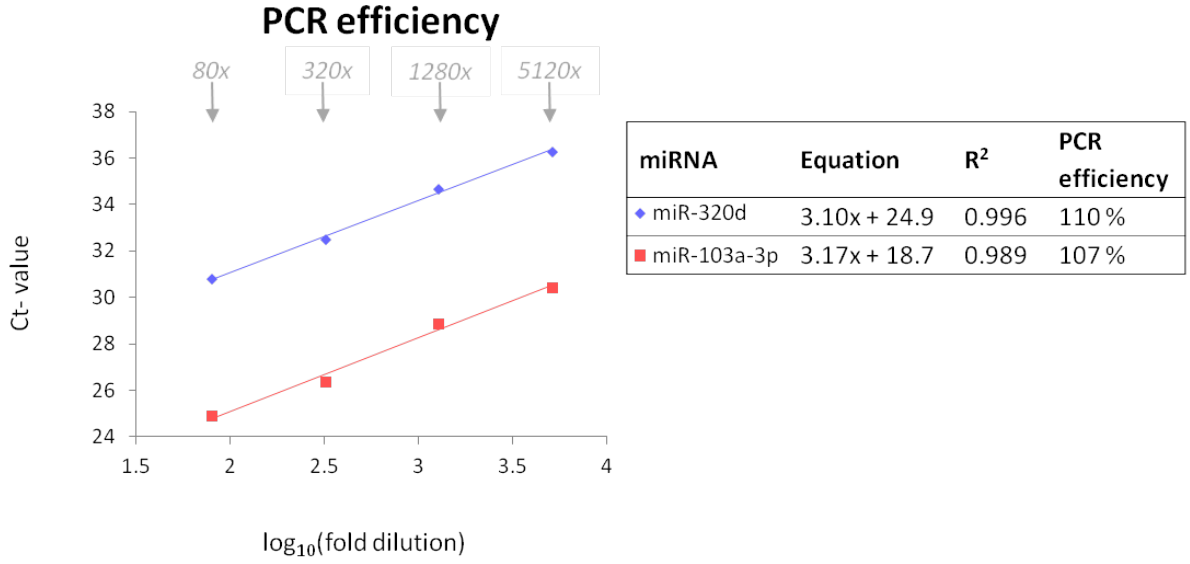

miRNA	Equation	R^2	PCR efficiency
miR-320d	3.10x + 24.9	0.996	110 %
miR-103a-3p	3.17x + 18.7	0.989	107 %

Figure 4.1: Serial dilutions of cDNA used to calculate the PCR efficiency for the primers corresponding to miR-320d and reference gene miR-103a-3p. Mean Ct values are plotted as functions of dilution on log-scale. The equation of the fitted curves and the corresponding PCR efficiencies are listed to the right.

4.2.2 Transfection with miR-320d mimic

In order to verify the transfection, and upregulation of miR-320d, total RNA was isolated from all transfection experiments, cDNA was synthesized, and then finally analyzed on RT-qPCR. The $2^{-\Delta\Delta Ct}$ method (Formula 2.1) was used for calculating the expression of miR-320d relative to the reference gene (miR-103a-3p). The upregulation worked successfully in all treated samples, but with highly variable fold inductions. The calculated mean gave 18 800 times upregulation in SiHa cells treated with miR-320d mimic, and 10 900 times upregulation in HeLa cells (Figure 4.2). Raw data can be found in Appendix 11.

.

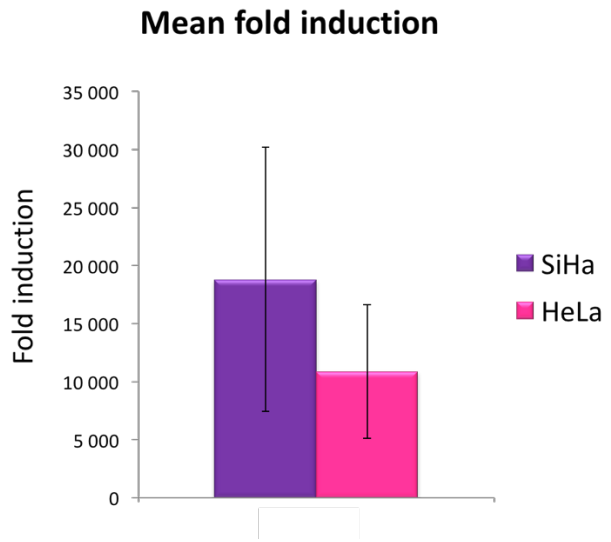

Figure 4.2: Fold induction of miR-320d in SiHa and HeLa cells treated with miR-320d mimics, relative to the endogenous levels of miR-320d in negative control cells. The data shown are mean ± SD of three individual experiments.

4.2.3 Melting curves

Melting curve analysis was done to identify the products from the RT-qPCR reaction, and thereby evaluate the purity of the product. By gradually increasing the temperature while monitoring the fluorescence from SYBR Green, it was possible to determine at which temperature the PCR products denatured, which could give indications of properties such as product size. Curves resulting from examination of the endogenous level of miR-320d in negative control samples showed one single peak at approximately 71 °C, indicating a pure product (Figure 4.3a). Melting curves resulting from samples treated with miR-320d mimics showed peaks at the same temperature, but with a higher derivative (Figure 4.3b). The derivative describes change in fluorescence, meaning that a high derivative corresponds to a large change in fluorescence, which is why mimic samples with overexpressed miR-320d have higher peaks than the negative controls. Additionally, jagged peaks were seen in front of the main peak, and to study what these could originate from, the PCR products were analyzed by electrophoresis.

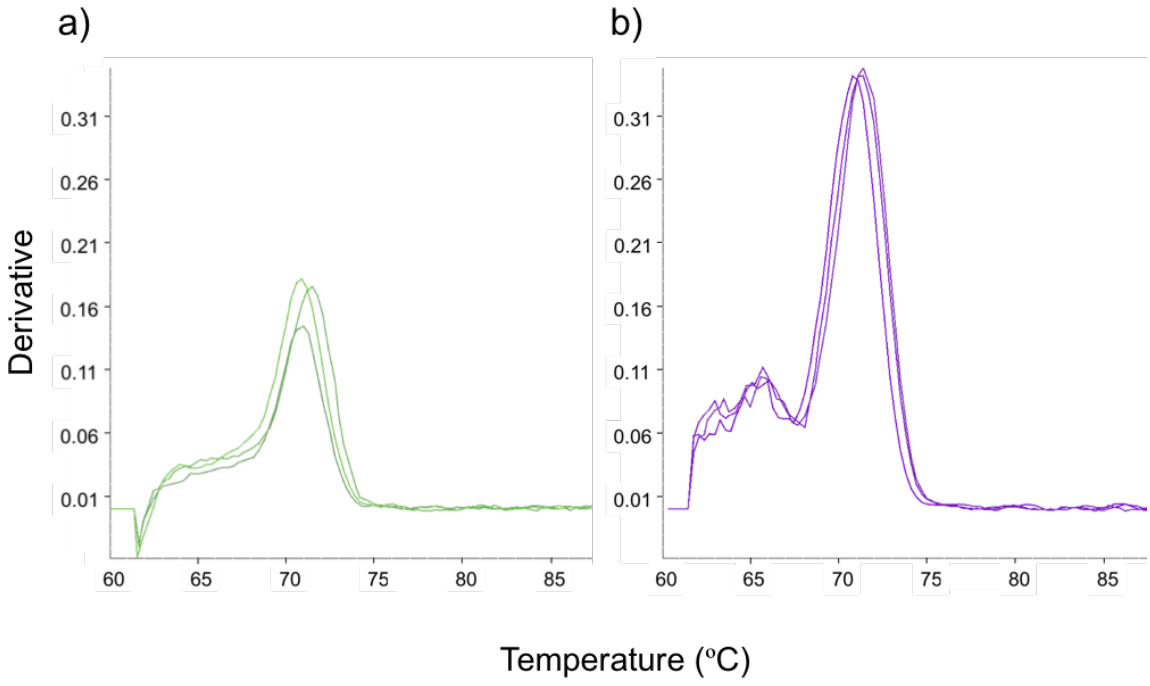

Figure 4.3: Melting curves of miR-320d PCR products resulting from a) negative control samples and b) samples treated with miR-320d mimics. Increasing temperature is shown along the x-axis and the derivative on the y-axis.

4.2.4 Size of the miR-320d PCR product

The PCR products resulting from miR-320d were sent to the Genomics Core Facility at the institute for analysis by electrophoresis (TapeStation), in which the PCR products are separated by size.

Figure 4.4 show that the PCR products were 47-48 bp long, represented by the largest peaks, colored in purple (SiHa cells) and pink (HeLa cells). Additional peaks at 42-43 bp were seen in the negative control from SiHa cells and both samples from HeLa cells. As these were not confined to samples treated with miR-320d mimic, they could not explain the feature seen in the melting curves. One possibility could be that these peaks originate from primer-dimers, but correspondence with the supplier of the primers and RT-qPCR kit (Exiqon) rejected this suggestion.

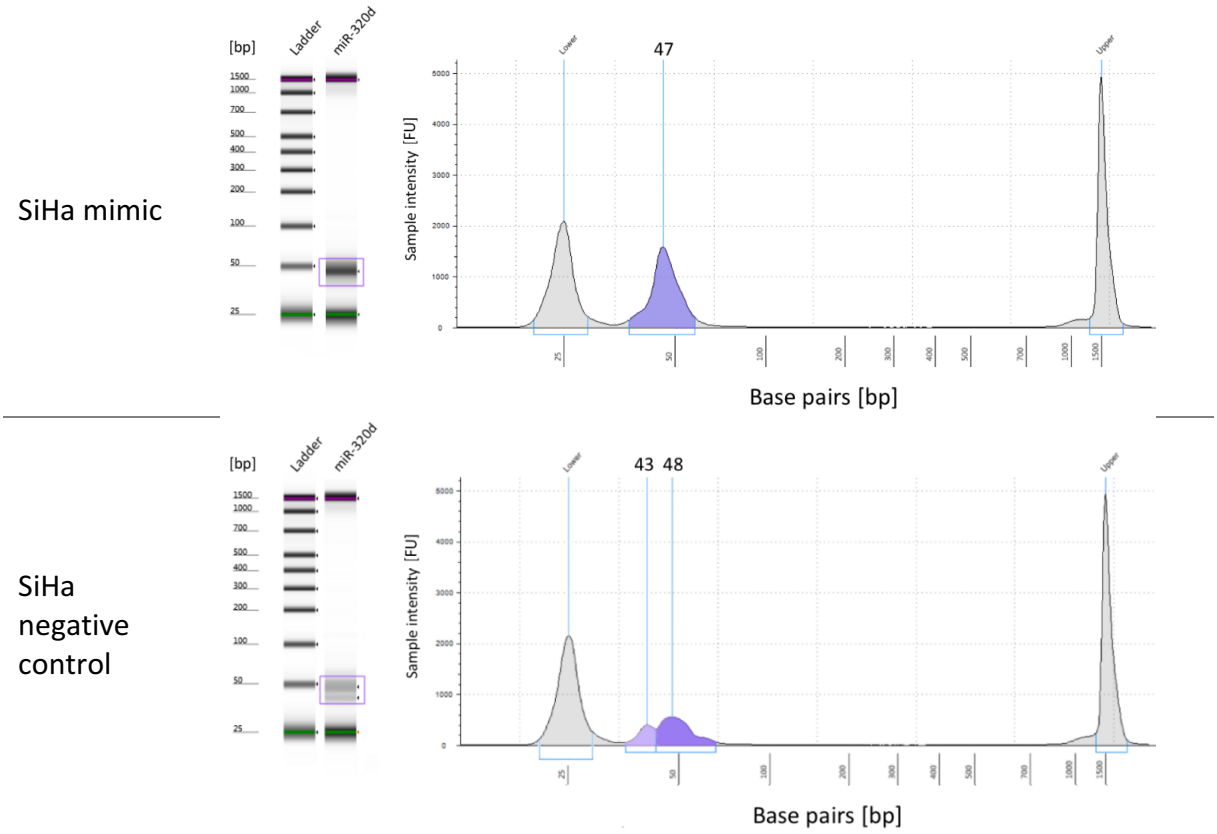

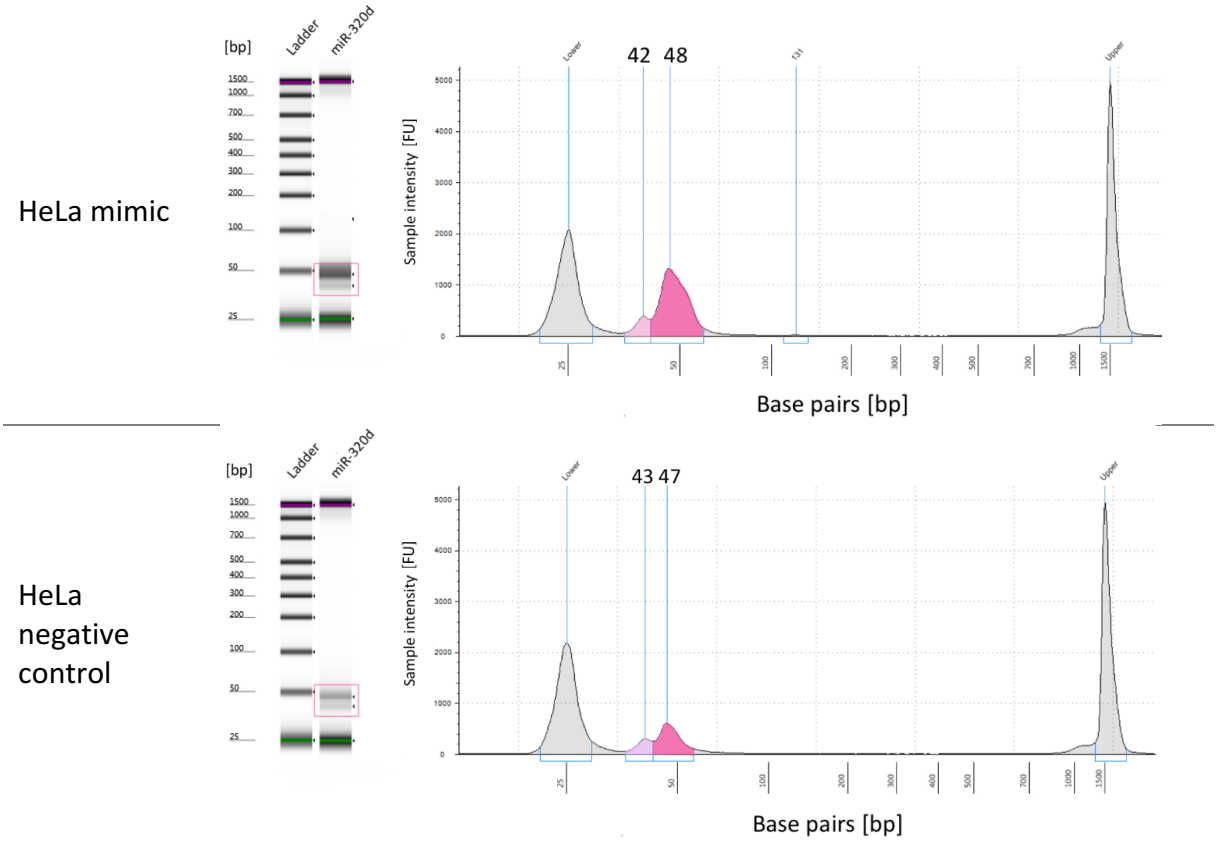

Figure 4.4: Left: Gels resulting from electrophoresis of PCR products. The ladders are used as references to estimate the size of the miR-320d PCR product, which is marked with a purple box for SiHa cells and a pink box for HeLa cells. Right: Electropherograms showing the separation done by electrophoresis. The size of the PCR product is estimated to be 47-48 bp. Additional byproducts, 42-43 bp in size, were also detected.

4.2.5 Transfection duration

To examine the duration of the miR-320d upregulation, the expression of miR-320d was measured for 10-12 days, depending on cell line. In order to have the same conditions for the cells throughout the experiment, the samples from day 0 were excluded as these resulted from harvest directly after the end of transfection (22 hours post-ransfection). Hence, the first data points included were from 46 hours post-transfection. The curves in Figure 4.5 illustrate the decay of miR-320d expression after upregulation with mimics for HeLa and SiHa cells. A steady decline was found for both cell lines, and the experiment was terminated after 10 days for HeLa and after 12 days for SiHa. The equations of the curves fitted to the data points were used to calculate the half-life of miR-320d for both cell lines (Formula 3.3), and found to be 56 hours in SiHa cells and 44 hours in HeLa cells. The half-lives were expected to roughly correspond with the doubling time of the cell lines, but based on previous knowledge[73], SiHa and HeLa cells doubles exceedingly faster than every 56th and 44th hour. Raw data can be found in Appendix 11.

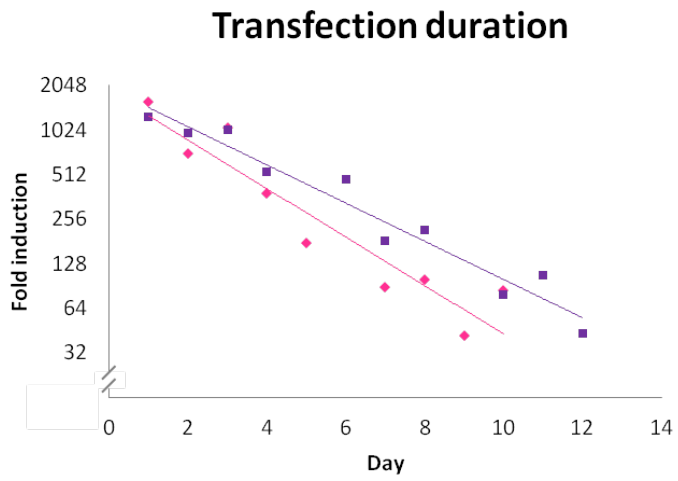

Cell line	Exponential function	miR-320d half-life, $t_{1/2}$ (hours)
HeLa	$1859\, e^{-0.377x}$	44
SiHa	$1952\, e^{-0.297x}$	56

Figure 4.5: Transfection duration for HeLa cells (10 days) and SiHa cells (12 days). The curve of HeLa cells is steeper than the curve of SiHa cells, meaning that the relative miR-320 level decreased faster in HeLa cells.

4.2.6 Duration of transfection in relation to cell proliferation

To better understand the unexpectedly slow decline of miR-320d expression with time after transfection, proliferation assays were performed to directly compare transfection duration with the proliferation rate in the model system. This was done to see if transfection decreased the doubling time. The curves in Figure 4.6a show the proliferation curves of mimic- and negative control treated SiHa and HeLa cells. Regression lines were fitted to the exponential phases of both curves (Figure 4.6b), and then used to find initial and final number of cells within the exponential phase (Table 4.2). For both cell lines, the exponential growth was seen between day 3 and 6. The doubling time for SiHa cells was calculated to be 25 hours for cells treated with miR-320d mimic and 27 hours for negative control cells (Formula 3.4). HeLa cells proliferated faster, and the doubling time was calculated to be 26 hours for cells with overexpression of miR-320d, and 27 hours for negative control cells. Neither of the cell lines showed significant difference between the negative control and mimic treated cells, and proliferation can therefore not explain the long duration of miR-320d overexpression in cells treated with this mimic. Raw data can be found in Appendix 12.

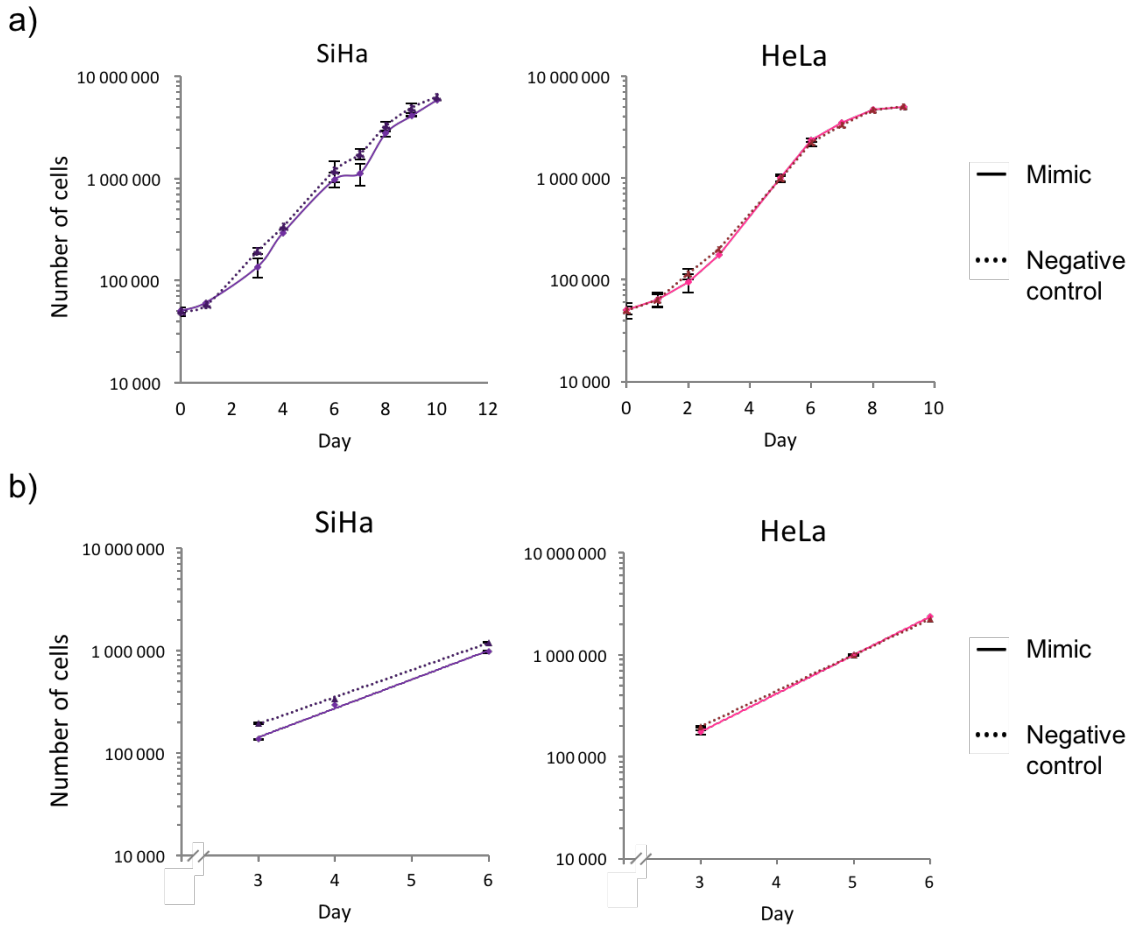

Figure 4.6: a) Counted number of cells plotted as a function of time (days) for SiHa and Hela cells treated with miR-320d mimic and their negative control. Each point is mean ± SD for triplicates within one experiment b) Regression of exponential phases of SiHa and HeLa proliferation curves. The resulting equations (not shown) were used to calculate the number of cells in Table 4.2.

Table 4.2: Cell doubling times calculated from the exponential phases of the growth curves. The numbers of cells at start and end of the exponential phase are found from the regression line shown in Figure 4.6b.

		Exponential phase, number of cells Start (N_0=day 3)	End (N_t=day 6)	**Doubling time (T_d), hours**
SiHa	Negative control	191 916	1 187 087	27
	Mimic	142 776	999 025	26
HeLa	Negative control	197 513	2 248 251	21
	Mimic	175 389	2 372 282	19

4.3 Biological effect of transfection with miR-320d mimic

4.3.1 Survival

To study whether increased levels of miR-320d affect cell survival, transfected cells were plated out for clonogenic assay. Figure 4.7 shows the plating efficiencies calculated from Formula 3.5. A significant decrease in cell survival was seen for SiHa cells transfected with miR-320d mimic compared to the negative control ($p = 0.0091$). For HeLa cells, the decrease was not significant ($p = 0.13$). Raw data can be found in Appendix 13.

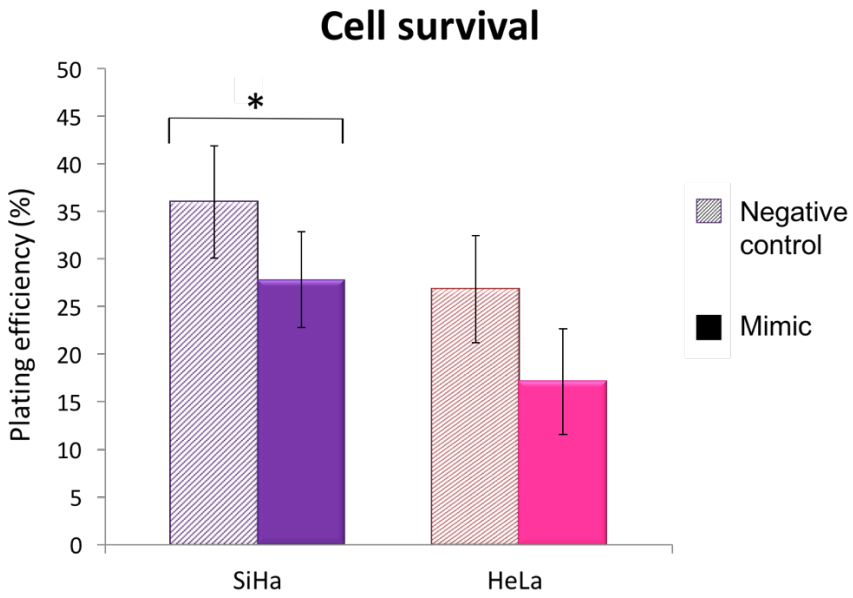

Figure 4.7: Cell survival shown as plating efficiency. Negative control cells are compared to cells transfected with miR-320d mimic, for SiHa and HeLa cells. The data shown are mean ± SD of three individual experiments (*$p < 0.05$).

4.3.2 Cell cycle distribution

The cell cycle distributions represented by typical DNA histograms are shown in Figure 4.8 while Figure 4.9 shows the mean of three individual experiments. Both cell lines showed highest fraction of cells in G_1 phase, lower in S phase and the lowest fraction of cells in G_2/M phase. It was not possible to distinguish between G_2 and M phase as the cells were stained with Hoechst. Statistical testing showed no significant difference in cell cycle distribution between negative control- and mimic treated cells. Raw data can be found in Appendix 14.

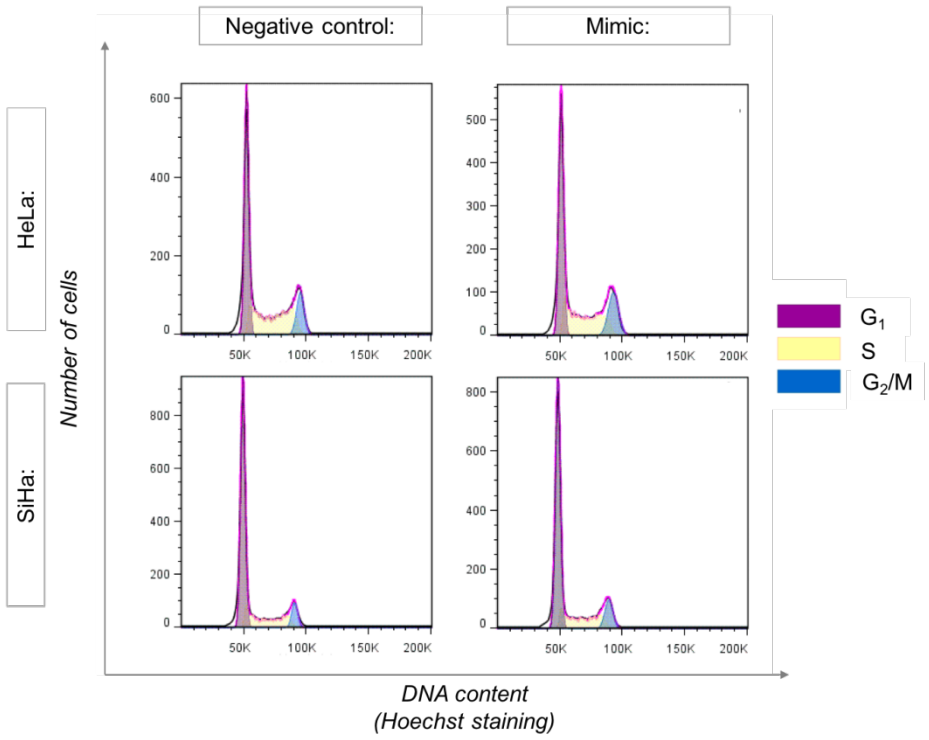

Figure 4.8: DNA histograms showing cell cycle distribution of HeLa and SiHa cells after treatment with negative control or miR-320d mimic, and with cells in G_1, S and G_2/M phase indicated with different colors. The histograms are made in FlowJo (software) and are representative of three separate experiments.

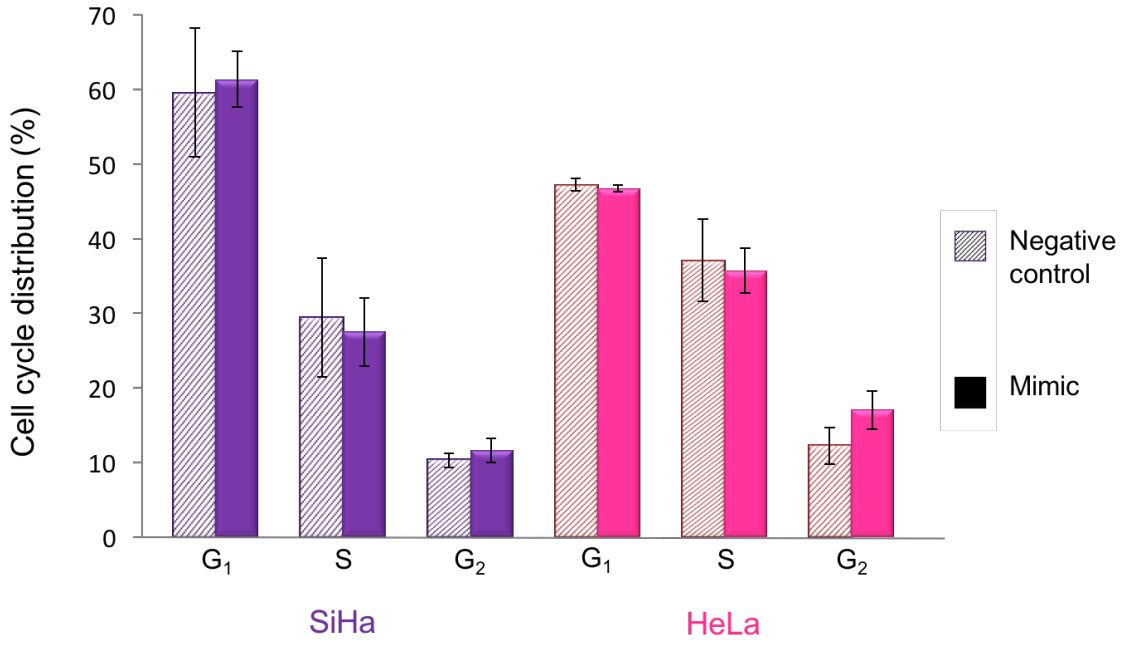

Figure 4.9: Calculated cell cycle distributions shown as mean ± SD of three individual experiments for SiHa and HeLa cells treated with miR-320d mimic and negative control. The values are normalized and shown as percentage distribution.

4.3.3 Apoptosis

To look for apoptosis, the cells were labeled with Cy5 using TUNEL assay and were then analyzed on the BD LSR II Flow cytometer. After separation of single cells from doublets, the Cy5 labeling was examined to separate non-apoptotic cells from apoptotic cells. The fraction of non-apoptotic cells was determined by gating the cells clustering at a relatively low Cy5 signal, corresponding to the lower cluster of cells seen in the positive control (Figure 4.10). MiR-320d overexpression did not show any increase or decrease of the apoptotic fractions in neither of the cell lines. Both negative controls and samples treated with miR-320d mimics had 1-2 % apoptotic cells, which is a negligible amount compared to the positive control with 28 % apoptotic cells (Figure 4.11). Raw data can be found in Appendix 15 15.

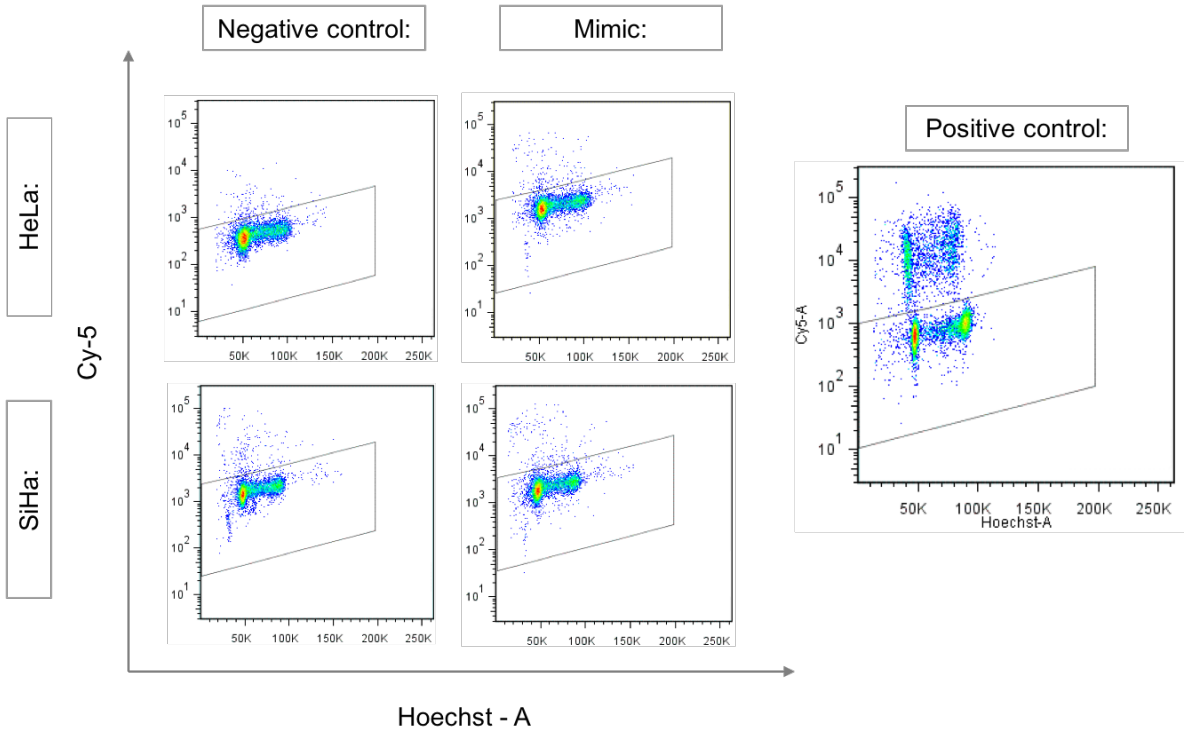

Figure 4.10: Representative dot plots of HeLa and SiHa cells treated with miR-320d mimic or negative control. The non-apoptotic fraction is gated into the grey boxes, leaving the apoptotic fractions outside. A positive control (Reh cells) show what a dot plot looks like if there is a large fraction of apoptotic cells present.

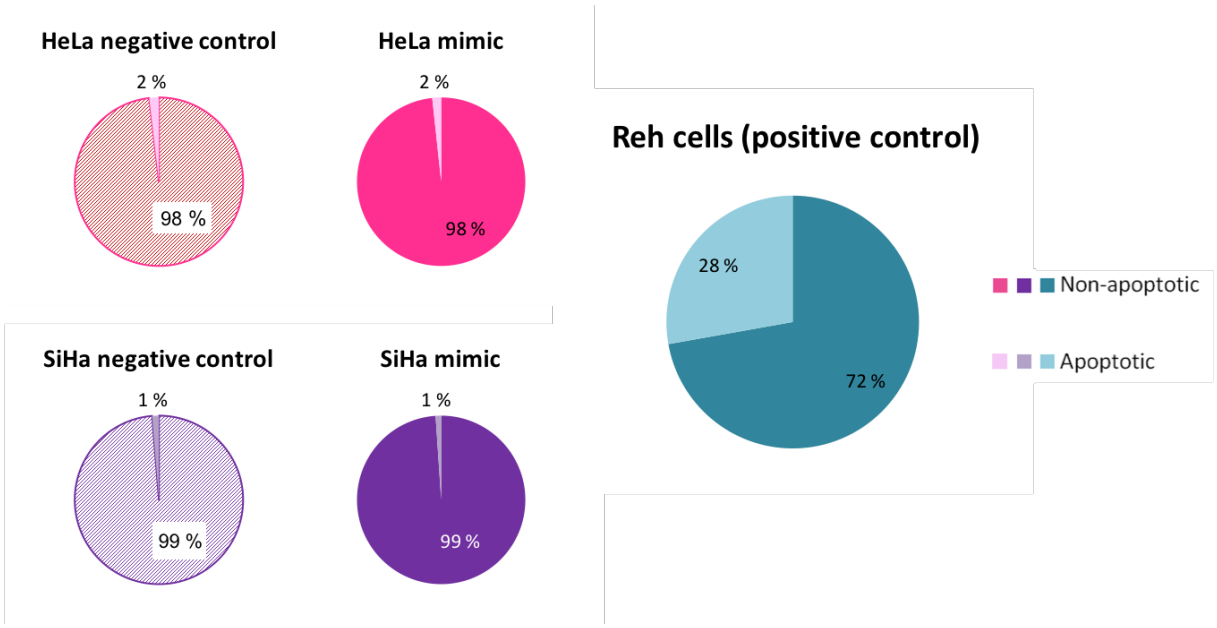

Figure 4.11: Pie charts showing non-apoptotic and apoptotic fractions resulting from TUNEL assay done on HeLa and SiHa cells treated with miR-320d mimic or negative control. An additional positive control (Reh cells) was included to see the distribution within a cell line known to have a large apoptotic fraction.

4.3.4 Radiosensitivity

To see whether miR-320d affect the radiosensitivity, transfected cells were irradiated and then plated out in clonogenic assays to examine the cell survival. The cells were irradiated with 2 Gy and 4 Gy, in addition to a non-irradiated sample (0 Gy). Survival fractions were calculated from Formula 3.6 for all samples and then normalized to the 0 Gy sample, and the normalized survival fractions were plotted against radiation dose in Figure 4.12. No difference between negative control and cells treated with miR-320d mimic was observed, meaning that there are no clear indications of the role of miR-320d alone in relation to radiosensitivity. Raw data can be found in Appendix 16.

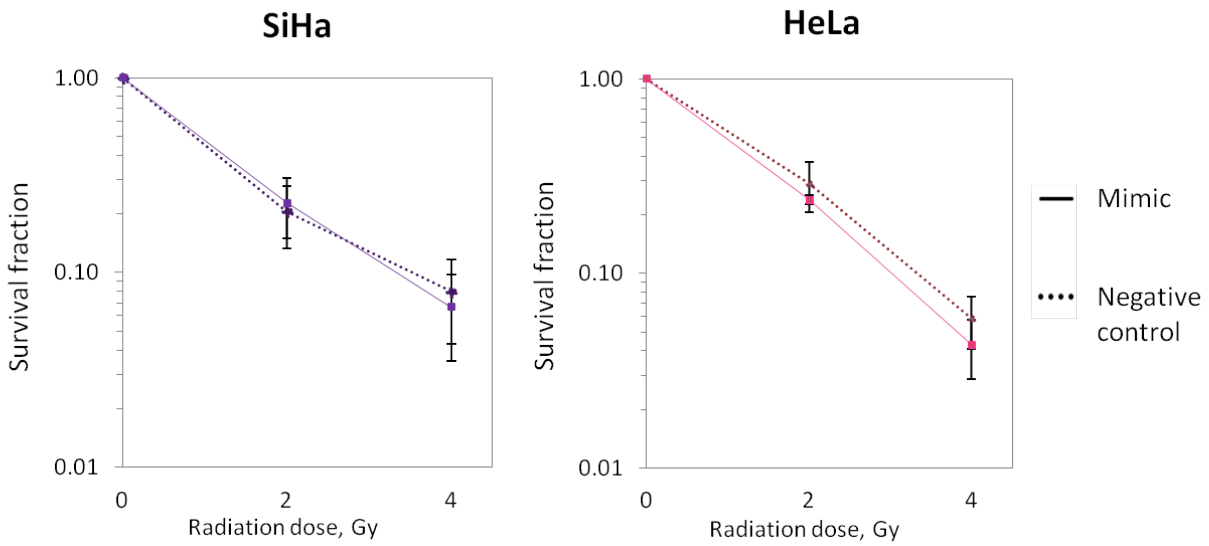

Figure 4.12: Radiation sensitivity of SiHa and HeLa cells treated with miR-320d mimic and negative control. The results show mean ± SD of three experiments, and no difference of significance was seen between mimic and negative control for any of the cell lines.

5 Discussion

Experimental considerations

SiHa and HeLa cervical carcinoma cell lines were used as model systems in the experiments. They were given the same optimal conditions for growth to make sure that differing temperature and supply of CO_2, oxygen and nutrients did not influence the results.

Tumor microenvironments are often very heterogeneous involving varying access to oxygen and nutrients, and can cause heterogeneous responses to cancer therapy such as irradiation. MiRNA profiles have also been found to be highly variable in both normal and cancerous tissues of the cervix[74]. Conflicting papers have been published, where a certain miRNA was found to be upregulated in one study[37] and downregulated in another[74]. Compared to a human tumor, the model systems are much more homogenous, and the results can therefore not be directly applied to human cervical cancers. Additionally, as the cell lines used have been cultured over a long period of time, they might have diverged somewhat from the tissue they originate from (cervix cancer) and the characteristics may have changed. However, the results obtained can be used to provide answers to individual questions regarding cancer cell behavior, and to set up hypotheses for human cancers.

Mir-320d was selected for studies of overexpression in HeLa and SiHa cells and miR-103a-3p was used as reference gene. RT-qPCR was the method used for measuring expression of these two miRNAs, and in order to find suitable cDNA dilutions for the RT-qPCR setup, the PCR efficiency for miR-320d and miR-103a-3p had to be calculated. Linear standard curves were made, and cDNA dilutions ranging from 80x to 5120x were found to be usable. Only non-treated HeLa cells were tested as the SiHa cells were found to behave similarly by having Ct values within the same ranges in pre-studies where primers for miR-320d and miR-103a-3p, were tested. The calculated PCR efficiencies (Formula 3.1) were within the range of what is considered as optimal (miR-320d: 110 %, miR-103a-3p: 107 %).

Melting curve analysis is a pre-programmed setting of the RT-qPCR program, and was performed for each PCR product. The melting curves seen for the different PCR products, both miR-320d and the reference gene miR-103a-3p, showed clean peaks indicating pure products during establishment and optimization of the RT-qPCR set-up. However, in the transfection experiments, additional noisy features looking like enlarged jagged peaks were seen in front of

the peaks corresponding to the miR-320d PCR product in the samples treated with miR-320d mimic. This feature was absent in the negative control, indicating that it could be caused by the mimic treatment rather than being a result of primer-dimers. Electrophoresis was done to look further into what these additional jagged peaks could result from. The main miR-320d PCR product was found to be 47-48 bp long, in addition to a minor product of 42-43 bp. However, the less abundant product was found in both the negative control and miR-320d mimic samples, and was therefore probably not related to the transfection. Compared to the peaks corresponding to the miR-320d PCR products in mimic treated samples, the jagged peaks in front was relatively small and was therefore considered to not affect the final result to a large extent. Possibly, they contributed to Ct values slightly lower than what they otherwise would have been, which result in slightly higher calculated fold inductions. This could have been a problem if we were looking at overexpression at lower magnitude, but as shown, the miR-320d mimics caused tremendous upregulations which could not mainly be caused by the byproduct alone.

RNA isolation and RT-qPCR analysis showed that cells were successfully transfected as the average levels of miR-320d were 18 800 (SiHa) and 10 900 (HeLa) times higher in the cells treated with miR-320d mimics than in the negative control cells. However, the upregulations in the individual experiments differed quite a lot, although they were all at least 5000 times upregulated. One reason for these differences could be that the method for calculating the fold induction (the $2^{-\Delta\Delta Ct}$ method, Formula 2.1) is very sensitive for variations in the Ct values, especially when there are large differences between the different samples, such as for the miR-320d mimic treated sample and the negative control.

Although RT-qPCR is a valid technique for analyzing the amount of miRNA, there are evidences showing that the supraphysiological levels resulting from transient transfection does not represent the actual levels of functional miRNA[75]. Thomson et al did additional immunoprecipitation and deep sequencing analyzes to determine the level of functional transfected miRNA. This showed that the analysis by the RT-qPCR method resulted in more than ten times higher upregulation than what was actually functional and bound to miRISC. Excessive miRNA was found to be localized with or in close proximity to lysosomes. These findings indicate that the levels of miR-320d in transfected SiHa and HeLa cells, found by RT-qPCR analysis, do not necessarily represent the functional levels, but are considerably higher.

Duration of the transfection was studied to see for how long the miR-320d mimic persisted in the cells. The large drop seen from day 0 to day 1 of the study can be caused by several reasons.

First, the washing step between the removal of transfection medium and cell lysis might affect the total amount of miR-320d mimic in the resulting cell lysate, and insufficient washing can cause upregulations above what is the real level. Cells seeded for analysis of transfection duration were washed more thoroughly than the cells harvested at day 0. Second, it is possible that the cells with the most extreme upregulation died, without immediately detaching from the surface, causing them to be included in the measurement of miR-320d at day 0, but not for the remaining days.

The transfection half-life in SiHa (56 h) was longer than in HeLa cells (44 h), which might be explained by the faster proliferation of HeLa compared to SiHa cells. However, even though HeLa normally proliferates faster than SiHa, both calculated half-lives were considerably longer than the cell doubling times previously found in the lab[73,76]. Because of this, it was decided that proliferation should be tested to see whether the treatment with miR-320d mimic caused a decrease in the doubling time of the cells. Previous studies have shown that high levels of miR-320d in diffuse large B-cell lymphomas can result in significantly decreased proliferation[39]. Here, we saw that treatment with miR-320d mimic of cervical cancer cell lines did not cause any significant differences in proliferation compared to the negative control in neither of the two cell lines. The experiment was only performed once, but based on previous knowledge about the cell division rates of HeLa and SiHa[73], there are reasons to believe that the results are reliable.

The doubling times of the transfected cells were 26-27 hours for SiHa and 19-21 hours for HeLa, which coincide with other studies done on proliferation[73, 76]. A cell doubling time of approximately the same as the half-life could have indicated that the cell division alone was responsible for the decrease of miR-320d, and a half-life shorter than the doubling time could have indicated an additional degradation. Eventually, if miR-320d lead to decreased proliferation, the lower cell doubling time could have been caused by non-transfected cells "taking over" the cell population by proliferating faster than cells transfected with miR-320d. This would have given a false impression about the doubling time. However, a doubling time considerably lower than the half-life of miR-320d was not expected, but was seen as the result of the transfection efficiency and proliferation experiment. These numbers are hard to explain, but one potential hypothesis, is that transfection with miR-320d activates some kind of positive feedback mechanism that causes an additional increase in the level of naturally occurring miR-320d. This could be mediated by a mechanism where miR-320d itself targets a transcriptional

repressor which downregulates miR-320d, but there are to date no published papers pointing in this direction.

The continuous decrease in miR-320d after overexpression by transient transfection caused limitations of the study of proliferation, as the amount of miR-320d changed during the experiment. For proliferation studies, stable transfection is therefore a better option. Survival measured using clonogenic assay was, on the other hand, more reliable. Even though the levels of miR-320d decreased when the cells divided in the colonies, the cells that were plated out in this assay had greatly increased levels of miR-320d from the very beginning, as they were plated out directly after transfection. This means that the colonies resulted from cells originally transfected. Even though the level of miR-320d in the individual cells of each colony decreased gradually, this did probably not affect the total number of colonies, which was used as the measurement of sustaining proliferative survival. Radiation was performed 22-hours post-transfection and immediately before seeding out for clonogenic assay, meaning that miR-320d was still highly overexpressed at this point. The cells were fixated for analysis of apoptosis and cell cycle distribution 22-46 hours post-transfection, meaning that also these cells had high levels of miR-320d.

Biological effects of overexpressing miR-320d

Upregulation of miR-320d turned out to significantly decrease the survival of SiHa cells under basal conditions, but not the HeLa cells. The decreased survival as a consequence of overexpression was consistent with the hypothesis of increased aggressiveness as a consequence of loss. Several studies have shown that miRNAs might play a role in the complex mechanism underlying radiosensitivity in different types of cancer[25]. However, there are currently no published studies on the relationship between miR-320d and radioresistance, neither in cervical cancer, nor in other cancer types. Because miR-320d is located within a region on chromosome 13q where loss is associated with radioresistance[1] in cervical cancer, it was of great interest to see whether this miRNA could be involved in the mechanism for radiosensitivity. Radiation experiments were performed by irradiating the cells with 2 Gy and 4 Gy, but no decrease in survival, meaning increase in radiosensitivity, was observed for SiHa or HeLa cells transfected with miR-320d. This was inconsistent with the hypothesis of increased radiosensitivity when miR-320d is overexpressed, and suggests that miR-320d alone cannot affect the radiosensitivity of the cells.

The cell cycle distribution was analyzed to examine whether the miR-320d mimic treatment resulted in cell cycle arrest in any specific phases. There are no published studies showing altered cell cycle distribution in cancer cells as a consequence of overexpressing miR-320d, but if a difference was to be seen, this could indicate a potential role of miR-320d in cell cycle progression. Flow cytometry analysis showed that the largest fraction of cells for both cell lines, independent on treatment, was in G_1 phase. SiHa cells had more G_1 cells than HeLa cells, but less S phase cells. Two of the experiments from each cell line were examined 22 hours post-transfection, and the third experiment was examined after 46 hours, as no difference was seen after 22 hours, but no difference in cell cycle distribution was observed in any of the cases. All samples analyzed was non-irradiated, meaning that the results obtained from this experiment cannot be used to say anything about the effect of miR-320d mimic combined with radiation.

Currently, there are no published studies showing increased apoptosis as a consequence of upregulation of miR-320d. However, a recent study on *MCL-1* in cervical cancer showed that miR-320 (not miR-320d specifically) may target the 3'-UTR of *MCL-1*[77]. *MCL-1* is involved in regulation of apoptosis in cancer cells[78], and by downregulating this mRNA, miR-320 can contribute to increased apoptosis. In this thesis, TUNEL assay was performed to look for differences in apoptotic fraction as a consequence of the treatment with miR-320d mimics. As for the cell cycle distribution analysis, two of the experiments were analyzed 22 hours post-transfection, and the third experiment was analyzed 46 hours post-transfection as no differences were observed in the 22 hour-samples. No difference was seen in miR-320d transfected SiHa or HeLa cells compared to the negative control. The results from the TUNEL assay itself were reliable, as the positive control cells (Reh cells) showed a markedly increased fraction of apoptotic cells compared to the SiHa and HeLa cells. Still, as for the cell cycle distribution analysis, all cells were non-irradiated, and the results can therefore not be used to give any information of the possible effect combined miR-320d mimic and irradiation has on apoptosis.

Even though the experiments in this thesis only showed that overexpression of miR-320d caused decreased cell survival in SiHa cells, it does not mean that miR-320d does not play a role in radioresistance in cervical cancer. Post-transcriptional miRNA regulation involves a complex system where one miRNA can target many different mRNAs, and also the targeting of one mRNA by many different miRNAs. Loss of miR-320d can possibly cause an aggressive phenotype by the combined effect of loss of several miRNAs and genes at 13q.

Future perspectives

A method for validating cell transfection with miR-320d mimics on RT-qPCR was established in this thesis. However, this method did not distinguish between functional miR-320d incorporated in miRISC and excessive miR-320d located elsewhere in the cells, which can explain the extreme upregulations found after transfection with mimics. A way of validating functional miRNAs introduced into the cell is by using luciferase assay, in which the fully complementary miRNA binding site is inserted in the 3' UTR of a luciferase gene within a vector called reporter plasmid. By co-transfecting the cells with the reporter plasmid in addition to the miRNA mimic, the functional expression level can be detected by measuring luciferase activity[79]. The more reduced luciferase activity is seen in the mimic-treated sample compared to the negative control sample, the more functional miRNA mimics is present. An alternative way to validate the level of functional miRNA mimics is immunoprecipitation followed by deep sequencing of miRNA bound to miRISC, as described in the paper published by Thomson et al[75].

Transfection efficiency, meaning to what extent the transfection worked successfully to introduce nucleic acids into the cells, was not tested in these experiments as there were no fluorescent labels on the miR-320d mimics ordered from Dharmacon. However, such verification of transfection should be considered in future studies. MiRNA mimics provided from Exiqon can be ordered with FAM labeling, which for instance is suitable for flow cytometry analysis.

Due to the limitations of transient transfection, stable transfection should be considered in future studies. In this thesis, the expression levels of miR-320d was found to be approximately 80 times upregulated in both cell lines by the time the proliferation assays were completed (after 8-10 days), which was 15-20 times lower than the expression levels at day 1. With stable transfection, miR-320d will be continuously overexpressed rather than being diluted as the cells divide, and the result from a proliferation assay will be more reliable. By having miR-320d integrated in the genome, it is also likely that RT-qPCR can be used to validate the actual levels of functional miR-320d rather than excessive mimics. Stable transfection can for instance be done by virus-mediated gene delivery (called transduction) for introducing a vector containing the gene encoding miR-320d. In addition to the gene, the delivered construct has to contain a selection marker which can be used for selecting transduced cells.

Only a selection of possible oncogenic processes was studied in this thesis. In future studies, the role of miR-320d in other processes such as migration and metabolism should also be considered. To further examine the role of miR-320d, it could be interesting to see if the effect seen on survival after overexpression in SiHa cells was the opposite after inhibition of miR-320d. This can be done using an inhibitor, preferably with a fluorescent tag, which binds to miR-320d and thereby prevents it from binding to its mRNA target. The consequence will be that more of the target mRNAs are translated into protein.

In order to get more insight into what regulatory role miR-320d plays in cervical cancer, we should proceed with studying altered gene expression after upregulation and/or inhibition of miR-320d. This will hopefully give candidate target genes of miR-320d, and thereby also indications of which biological processes miR-320d potentially regulates. Eventually, this information can be used for studies focusing on experimental validation of predicted mRNA targets. However, the complex system of interactions with multiple targets and regulators for the same miRNA and mRNA, respectively, makes the target validation for one specific miRNA challenging. In all likelihood, miR-320d is only one piece of a complex network of interacting miRNAs.

References

1. Lando, M., Holden, M., et al., *Gene dosage, expression, and ontology analysis identifies driver genes in the carcinogenesis and chemoradioresistance of cervical cancer.* PLoS Genet, 2009. **5**(11): p. e1000719.

2. Pecorino, L., *Molecular Biology of Cancer*. 3rd ed. 2012, Oxford, UK: Oxford University Press.

3. Alberts, B., *Molecular Biology of the Cell*. 5th ed. 2008: Garland Science.

4. Forman, D., Ferlay, J., *The global and regional burden of cancer*, in *World Cancer Report 2014*, B.W. Stewart, Wild C. P., Editor. 2014, World Health Organization. p. 29-31.

5. Kreftregisteret. *Antall nye tilfeller fordelt på primær lokalisasjon og kjønn - 2014*. [cited 2016 05.05]; Available from: http://www.kreftregisteret.no/no/Registrene/Kreftstatistikk/.

6. Eifel, P.J., *Concurrent chemotherapy and radiation therapy as the standard of care for cervical cancer.* Nat Clin Pract Oncol, 2006. **3**(5): p. 248-55.

7. Lowy, D.R., Schiller, J.T., *Reducing HPV-associated cancer globally.* Cancer Prev Res (Phila), 2012. **5**(1): p. 18-23.

8. Haverkos, H., Rohrer, M., et al., *The cause of invasive cervical cancer could be multifactorial.* Biomedicine & Pharmacotherapy, 2000. **54**(1): p. 54-59.

9. Calin, G.A., Sevignani, C., et al., *Human microRNA genes are frequently located at fragile sites and genomic regions involved in cancers.* Proc Natl Acad Sci U S A, 2004. **101**(9): p. 2999-3004.

10. CancerResearchUK.com. *Types of cervical cancer*. 2014 [cited 2016 10.04]; Available from: http://www.cancerresearchuk.org/about-cancer/type/cervical-cancer/.

11. Berrington, d.G.A., Green, J., *Comparison of risk factors for invasive squamous cell carcinoma and adenocarcinoma of the cervix: collaborative reanalysis of individual data on 8,097 women with squamous cell carcinoma and 1,374 women with adenocarcinoma from 12 epidemiological studies.* International journal of cancer. Journal international du cancer, 2007. **120**(4): p. 885-891.

12. Harvard Health, *Cervical polyps*. 2012: http://www.health.harvard.edu/womens-health/cervical-polyps.

13. Cannistra, S.A., Niloff, J.M., *Cancer of the uterine cervix.* N Engl J Med, 1996. **334**(16): p. 1030-8.

14. Pecorelli, S., *Revised FIGO staging for carcinoma of the vulva, cervix, and endometrium.* Int J Gynaecol Obstet, 2009. **105**(2): p. 103-4.

15. Sundfør, K. *Primær stråleterapi ved livmorhalskreft*. Oncolex 2012; Available from: http://www.oncolex.no/GYN/Diagnoser/Livmorhals/.

16. Crick, F., *Central dogma of molecular biology.* Nature, 1970. **227**(5258): p. 561-3.

17. Hanahan, D., Weinberg, R.A., *Hallmarks of cancer: the next generation.* Cell, 2011. **144**(5): p. 646-74.

18. Scheurer, M.E., Tortolero-Luna, G., et al., *Human papillomavirus infection: biology, epidemiology, and prevention.* Int J Gynecol Cancer, 2005. **15**(5): p. 727-46.

19. Ghittoni, R., Accardi, R., et al., *Role of human papillomaviruses in carcinogenesis.* Ecancermedicalscience, 2015. **9**: p. 526.

20. Ganguly, N., Parihar, S.P., *Human papillomavirus E6 and E7 oncoproteins as risk factors for tumorigenesis.* J Biosci, 2009. **34**(1): p. 113-23.

21. Chesson, H.W., Dunne, E.F., et al., *The estimated lifetime probability of acquiring human papillomavirus in the United States.* Sex Transm Dis, 2014. **41**(11): p. 660-4.

22. Weinberg, R.A., *The Biology of Cancer*. Second ed. 2014: Garland Science.

23. Kozomara, A., Griffiths-Jones, S., *miRBase: annotating high confidence microRNAs using deep sequencing data.* Nucleic Acids Research, 2014. **42**(D1): p. D68-D73.

24. Berezikov, E., Guryev, V., et al., *Phylogenetic Shadowing and Computational Identification of Human microRNA Genes.* Cell, 2005. **120**(1): p. 21-24.

25. Pedroza-Torres, A., López-Urrutia, E., et al., *MicroRNAs in Cervical Cancer: Evidences for a miRNA Profile Deregulated by HPV and Its Impact on Radio-Resistance.* Molecules, 2014. **19**(5): p. 6263-6281.

26. Sedani, A., Cooper, D.N., et al., *An emerging role for microRNAs in NF1 tumorigenesis.* Human genomics, 2012. **6**: p. 23.

27. Chendrimada, T.P., Gregory, R.I., et al., *TRBP recruits the Dicer complex to Ago2 for microRNA processing and gene silencing.* Nature, 2005. **436**(7051): p. 740-4.

28. Sigma-Aldrich, *miRNA Pathway*. 2015: http://www.sigmaaldrich.com/life-science/functional-genomics-and-rnai/mirna/learning-center/mirna-introduction.html.

29. Vasudevan, S., Tong, Y., et al., *Switching from repression to activation: microRNAs can up-regulate translation.* Science, 2007. **318**(5858): p. 1931-4.

30. Stahlhut, C., Slack, F.J., *MicroRNAs and the cancer phenotype: profiling, signatures and clinical implications.* Genome medicine, 2013. **5**(12): p. 111.

31. Jansson, M.D., Lund, A.H., *MicroRNA and cancer.* Molecular Oncology, 2012. **6**(6): p. 590-610.

32. Lee, R.C., Feinbaum, R.L., et al., *The C. elegans heterochronic gene lin-4 encodes small RNAs with antisense complementarity to lin-14.* Cell, 1993. **75**(5): p. 843-54.

33. Wightman, B., Ha, I., et al., *Posttranscriptional regulation of the heterochronic gene lin-14 by lin-4 mediates temporal pattern formation in C. elegans.* Cell, 1993. **75**(5): p. 855-62.

34. Lee, R.C., Ambros, V., *An extensive class of small RNAs in Caenorhabditis elegans.* Science, 2001. **294**(5543): p. 862-4.

35. Lagos-Quintana, M., Rauhut, R., et al., *Identification of novel genes coding for small expressed RNAs.* Science, 2001. **294**(5543): p. 853-8.

36. Lau, N.C., Lim, L.P., et al., *An abundant class of tiny RNAs with probable regulatory roles in Caenorhabditis elegans.* Science, 2001. **294**(5543): p. 858-62.

37. Lee, J.W., Choi, C.H., et al., *Altered MicroRNA expression in cervical carcinomas.* Clin Cancer Res, 2008. **14**(9): p. 2535-42.

38. Hu, X., Schwarz, J.K., et al., *A microRNA expression signature for cervical cancer prognosis.* Cancer Res, 2010. **70**(4): p. 1441-8.

39. Wu, P.Y., Zhang, X.D., et al., *Low expression of microRNA-146b-5p and microRNA-320d predicts poor outcome of large B-cell lymphoma treated with cyclophosphamide, doxorubicin, vincristine, and prednisone.* Hum Pathol, 2014. **45**(8): p. 1664-73.

40. Schepeler, T., Reinert, J.T., et al., *Diagnostic and prognostic microRNAs in stage II colon cancer.* Cancer Res, 2008. **68**(15): p. 6416-24.

41. Godfrey, A.C., Xu, Z., et al., *Serum microRNA expression as an early marker for breast cancer risk in prospectively collected samples from the Sister Study cohort.* Breast Cancer Res, 2013. **15**(3): p. R42.

42. Zhi, F., Cao, X., et al., *Identification of circulating microRNAs as potential biomarkers for detecting acute myeloid leukemia.* PLoS One, 2013. **8**(2): p. e56718.

43. Hall, E.J., *The Physics and Chemistry of Radiation Absorption*, in *Radiationbiology for the Radiationbiologist*, J.-R. John, et al., Editors. 2000, Lippincott Williams & Wilkins: Philadelphia, USA.

44. Metheetrairut, C., Slack, F.J., *MicroRNAs in the Ionizing Radiation Response and in Radiotherapy.* Current opinion in genetics & development, 2013. **23**(1): p. 12-19.

45. RadiologyInfo.org. *Introduction to Cancer Therapy (Radiation Oncology)*. 2015 [cited 2016 14.05.16]; Available from: http://www.radiologyinfo.org/en/info.cfm?pg=intro_onco.

46. Liu, S., Pan, X., et al., *MicroRNA-18a enhances the radiosensitivity of cervical cancer cells by promoting radiation-induced apoptosis.* Oncol Rep, 2015. **33**(6): p. 2853-62.

47. Ye, C., Sun, N.X., et al., *MicroRNA-145 contributes to enhancing radiosensitivity of cervical cancer cells.* FEBS Lett, 2015. **589**(6): p. 702-9.

48. Yuan, W., Xiaoyun, H., et al., *MicroRNA-218 enhances the radiosensitivity of human cervical cancer via promoting radiation induced apoptosis.* Int J Med Sci, 2014. **11**(7): p. 691-6.

49. The Royal College of Radiobiologists, *Guidance on radiotherapy dose-fractionation*, in *Radiorherapy Dose-Fractionation*. 2006, The Royal College of Radiologists. p. 36-37.

50. Brown, T.A., *The Polymerase Chain Reaction (PCR)*, in *Genomes 3*. 2007, Garland Science Publishing. p. p. 56-57.

51. Livak, K.J., Schmittgen, T.D., *Analysis of relative gene expression data using real-time quantitative PCR and the 2(-Delta Delta C(T)) Method.* Methods, 2001. **25**(4): p. 402-8.

52. Bio-Rad Laboratories, *Real-Time PCR Applications Guide*. 2006.

53. Sean Taylor, Michael Wakem, et al., *A Practical Approach to RT-qPCR — Publishing Data That Conform to the MIQE Guidelines.* Bulletin, 2009.

54. Exiqon, *Locked Nucleic Acid (LNA) - Custom Oligonucleotides for RNA and DNA Research*. 2009: http://www.exiqon.com/ls/Documents/Scientific/LNA_folder.pdf.

55. Exiqon, *Screenshot from LNA Animation*. http://www.exiqon.com/.

56. Pryor, R.J., Wittwer, C.T., *Real-time polymerase chain reaction and melting curve analysis.* Methods Mol Biol, 2006. **336**: p. 19-32.

57. Exiqon, *miRCURY LNA Universal RT microRNA - Instruction manual*. 2015, http://www.exiqon.com/.

58. Exiqon, *miRCURY LNA Universal RT microRNA* 2015: Exiqon - Instruction manual.

59. Promega, *Transfection*. 2013: https://no.promega.com/resources/product-guides-and-selectors/protocols-and-applications-guide/transfection/.

60. Dharmacon. *miRIDIAN microRNA mimic* 2015; Available from: http://dharmacon.gelifesciences.com/microrna/miridian-microrna-mimic/.

61. Small, E.M., Olson, E.N., *Pervasive roles of microRNAs in cardiovascular biology*, in *Nature*. 2011, Nature Publishing Group, a division of Macmillan Publishers Limited. All Rights Reserved. p. 336-342.

62. BD Biosciences, *Introduction to Flow Cytometry: A Learning Guide*. 2000: http://www.d.umn.edu/~biomed/flowcytometry/introflowcytometry.pdf.

63. Faculty of Medicine and Dentistry - University of Alberta, *What is flow cytometry?* http://flowcytometry.med.ualberta.ca/.

64. Bortner, C.D., Oldenburg, N.B.E., et al., *The role of DNA fragmentation in apoptosis.* Trends in Cell Biology, 1995. **5**(1): p. 21-26.

65. Nagata, S., Nagase, H., et al., *Degradation of chromosomal DNA during apoptosis.* Cell Death Differ, 2003. **10**(1): p. 108-116.

66. ThermoFisher, *Cy®5 dye*. 2015: https://www.thermofisher.com/no/en/home/life-science/cell-analysis/fluorophores/cy5-dye.html.

67. ThermoFisher, *Hoechst 33258*. 2015: https://www.thermofisher.com/order/catalog/product/H21491?ICID=search-product.

68. ATCC, *HeLa (ATCC CCL-2)*. 2014: http://www.lgcstandards-atcc.org/products/all/CCL-2.aspx?geo_country=no - generalinformation.

69. ATCC, *SiHa (ATCC HTB-35)*. 2014: http://www.lgcstandards-atcc.org/Products/All/HTB-35.aspx.

70. QIAGEN, *miRNeasy Mini Handbook*. 2013.

71. Franken, N.A., Rodermond, H.M., et al., *Clonogenic assay of cells in vitro.* Nat Protoc, 2006. **1**(5): p. 2315-9.

72. ThermoFisher.com, *Fluorescence Spectra Viewer*. 2015: https://www.thermofisher.com/no/en/home/life-science/cell-analysis/labeling-chemistry/fluorescence-spectraviewer.html.

73. Caspersen, E.F., *Cell cycle distribution and CKS2 protein content in cervical carcinoma cell lines after exposure to ionizing radiation*, in *Rikshospitalet-Radiumhospitalet Medical Centre*. 2006, University of Oslo.

74. Pereira, P.M., Marques, J.P., et al., *MicroRNA Expression Variability in Human Cervical Tissues.* PLoS ONE, 2010. **5**(7): p. e11780.

75. Thomson, D.W., Bracken, C.P., et al., *On Measuring miRNAs after Transient Transfection of Mimics or Antisense Inhibitors.* PLoS ONE, 2013. **8**(1): p. e55214.

76. De Schutter, T., Andrei, G., et al., *Reduced tumorigenicity and pathogenicity of cervical carcinoma SiHa cells selected for resistance to cidofovir.* Molecular Cancer, 2013. **12**(1): p. 1-16.

77. Zhang, T., Zou, P., et al., *Down-regulation of miR-320 associated with cancer progression and cell apoptosis via targeting Mcl-1 in cervical cancer.* Tumour Biol, 2016.

78. Harrison, L.R., Micha, D., et al., *Hypoxic human cancer cells are sensitized to BH-3 mimetic-induced apoptosis via downregulation of the Bcl-2 protein Mcl-1.* J Clin Invest, 2011. **121**(3): p. 1075-87.

79. Barbara Robertson, Allison St. Amand, et al., *Modulating endogenous microRNA targets with miRIDIAN™ microRNA Mimics and Inhibitors: miR-122 in hepatocarcinoma cells (Huh-7)*. 2014: Dharmacon - Application Note.

Appendix

*Appendix 1:**Splitting cells***

1. Heat cell culturing medium, PBS and trypsin to 37°C.

The procedure should be performed in an aseptic LAF bench.

2. Remove the cell medium and wash with PBS.
3. Add trypsin to detach the cells from the flask. See volume of trypsin in Table A1. Place the flasks into the incubator as the detachment takes a couple of minutes.
4. Inactivate the trypsin by adding cell culturing medium once the cells have detached. See volume of medium in Table A1.
5. Pipet up and down a couple of times to ensure a proper distribution of the cells.
6. Add the cell suspension to a new T_{75} flask (or continue to experiment).
    - 1-2 ml, depending on cell confluence, cell type and days before next splitting
7. Add fresh cell culturing medium to the cells (~10 mL)
8. Incubate the flasks in an incubator with humidified atmosphere containing 5% CO_2 and tempered to 37°C.

Table A1: Volumes for trypsination and inactivation

		Trypsin (mL)	Medium (mL)
T_{75}	HeLa	1	9
	SiHa	2	8
6-well plate	HeLa	0.5	2.5
	SiHa	1	2

Appendix 2: ***Protocol for purification of total RNA***

Done by using the miRNeasy Mini Kit according to the manufacturer's instruction (QIAGEN)

1. Remove cell culture medium and continue to direct lysis.
2. Add 700 µl QIAzol Lysis Reagent to each well. Use a cell scrape to collect the lysate.
3. Transfer the cell lysate to a 1.5 mL tube. Homogenize by vortexing.
   The procedure can be transiently stopped here. If so, place the lysates on ice.
   The homogenized cell lysate can be stored at – 70 °C for several months.

4. Leave the homogenate at room temperature for 5 min.
   If the homogenate have been stored at - 80°C, thawing should be performed quickly in a 37°C water bath.
5. Add 140 µL chloroform to the homogenate. Cap the tube and shake vigorously for 15 s to mix it.
6. Leave the tube at room temperature for 2-3 min.
7. Centrifuge at 12 000 g, 4 °C, for 15 min. The centrifugation should separate the sample into three phases. The upper, aqueous phase contains the RNA.
8. Transfer the upper phase carefully into new 1.5 mL tubes.
9. Add 1.5 volumes 100 % ethanol and pipet up and down to mix it.
10. Pipet up to 700 µL of the sample into an RNeasy Mini spin column placed in a 2 mL collection tube. Put the lid on and centrifuge at ≥ 8000 g for 15 s. Discard the flow-through.
11. Repeat step 10 if more of the sample remains.

<u>Washing procedure</u>

12. Add 700 µL Buffer RWT to the RNeasy Mini spin column. Put on the lid and centrifuge at ≥ 8000 g for 15 s. Discard flow-through.
13. Add 500 µL Buffer RPE to the RNeasy Mini spin column. Put on the lid and centrifuge at ≥ 8000 g for 15 s. Discard flow-through.
14. Add 500 µL Buffer RPE to the RNeasy Mini spin column. Put on the lid and centrifuge at ≥ 8000 g for 2 min. Discard the collection tube containing the flow-through.
15. Place the RNeasy Mini spin column into a new 2 mL collection tube and centrifuge at maximum speed for 1 min.

Elution

16. Place the RNeasy Mini spin column into a new 1.5 mL collection tube. Add 30 µL RNase-free water to the column. Put the lid carefully on and centrifuge at ≥ 8000 g for 1 min to elute the RNA.
17. Repeat step 16 if expected yield exceeds 30 µg. The RNA can be eluted into the same tube.
18. Measure the RNA concentration at NanoDrop and store the isolated RNA at – 80 °C.

Appendix 3: ***Protocol for cDNA synthesis/reverse transcription***

Following the miRCURY LNA™ Universal RT microRNA PCR protocol from Exiqon

NB: Keep the reagents and reactions on ice at all times.

1. Adjust each of the template RNA samples to a concentration of 5 ng/µl by using nuclease-free water.
2. Gently thaw 5x reaction buffer, synthetic RNA spike-ins and nuclease-free water. Mix the reaction buffer by vortexing and the RNA spike-ins by gently flicking the tube. Place the reactants on ice. The enzyme mix should be kept at – 20 °C for as long as possible.

The reagents in the following steps can be made as a master mix if the first strand cDNA synthesis is to be performed on multiple RNA samples. The enzyme/template volume is replaced by nuclease-free water in the controls.

Volumes of one RT reaction:

	Reagent	**Volume (µL)**
RT working solution	Nuclease-free water	4.5
	5x Reaction buffer	2
	Synthetic RNA spike-ins	0.5
	Enzyme mix	1
	Template total RNA (5 ng/µL)	2
	Total volume	*10*

3. Make a reverse transcription (RT) working solution by mixing nuclease-free water, reaction buffer, RNA spike-ins and enzyme mix. Add the enzyme mix last to avoid a potentially premature reaction. Gently pipet up and down.
4. Dispense the RT working solution into nuclease-free tubes suitable for the PCR machine.
5. Add the diluted RNA template (5 ng/µL) and mix by pipetting up and down or by gentle vortexing. Spin down to avoid bubbles.
6. Perform the reverse transcription by using the following settings on the thermal cycler:

	Step 1	**Step 2**	**Step 3**
Temperature (°C)	42	95	4
Time (min.)	60	5	∞

7. Store the cDNA at 4 °C (up to four days) or freeze at -20 °C (up to 5 weeks).

Appendix 4: ***Protocol for qPCR***

1. Thaw cDNA, nuclease-free water and 2x PCR Master mix on ice for 15-20 min. The PCR Master mix should be protected from light.
2. Mix the cDNA by vortexing and dilute 240x in nuclease-free water.
3. Make a master mix containing 2x PCR Master mix, nuclease-free water and ROX for all reactions:

   Volumes of <u>one reaction</u>:

Reagent	**Volume (µL)**
2x PCR Master mix	5
Nuclease-free water	0.9
ROX	0.1
Total volume	*6*

4. Make a working solution for each primer.

   Volumes of <u>one reaction</u>:

Reagent	**Volume (µL)**
Master mix	6
PCR primer mix	1
Total volume	*7*

5. Add the master mix to each well.
6. Add 3 µL 240x cDNA to each well and mix the reactions by gently pipetting. The final concentration of the cDNA is now 320x.
7. Seal the plate with optical sealing and spin down in a centrifuge at 1500 g for 1 min.
8. Set up the contents of each well in the software, such as SDS.
9. Perform the amplification followed by melting curve analysis by using the following settings:

Step	**Settings**
Polymerase activation/denaturation	95°C, 10 min
Amplification	40 cycles: 95°C, 10 s 60°C, 1 min
Melting curve analysis	Yes

Appendix 5: ***Protocol for the mimic transfection experiment***

DAY 1

1. Count cells and plate the number that will reach confluence after two days.

   Volumes to be plated:

   $$HeLa: \frac{300\ 000}{x\ cells\ per\ mL} = mL\ cell\ suspension$$

   $$SiHa: \frac{625\ 000}{x\ cells\ per\ mL} = mL\ cell\ suspension$$

DAY 2

2. Replace culture medium with 2 mL antibiotic- and serum free medium (SFM) one hour before transfection.
3. Prepare a DharmaFECT/SFM-mix.

   For one well in a 6-well plate:

   196 µL SFM + 4 µL DharmaFECT transfection reagent

   Mix by pipetting carefully up and down.

   Leave at room temperature for 5 min.
4. Prepare a Mimic/SFM-mix.

   For one well in a 6-well plate:

   170 µL SFM + 30 µL Mimic (5 µM)
5. Carefully transfer the Mimic-SFM mix drop-wise to the DharmaFECT/SFM mix.

   Mix by pipetting up and down. Avoid air bubbles.

   Incubate at room temperature for 20 minutes.
6. Refresh the medium on the cells with 1.6 mL antibiotic free medium (AFM).
7. Transfer the DharmaFECT/Mimic mix to the cells.
8. Incubate for 22 hours at 37°C, 5 % CO_2.

DAY 3

9. Refresh medium with complete culture medium or harvest cells.

Appendix 6: ***Protocol for the growth curve experiment***

1. Perform splitting of cells as described in the steps 1-6 in appendix 1(Protocol for cell splitting).
2. Measure the number of cells per mL cell suspension by using a coulter counter.
3. Calculate the volume that corresponds to the predetermined number of cells.
4. Seed out the calculated volume into T_{25}-flasks. The number of flasks should be sufficient for three parallels to be measured every day.
5. Add 5 mL preheated medium to each flask.
6. Put the flasks in an incubator containing 37°C humidified atmosphere with 5 % CO_2.

Counting

7. Heat cell culture medium, PBS and trypsin in a heat bath until the temperature is about 37 °C.
8. Remove the old medium and wash with 1-2 mL PBS
9. Add trypsin and put the cell culture flask into the incubator for a couple of minutes until the cells have detached. Knocking carefully on the side of the flask will help the detachment.
    - SiHa: 1 mL
    - HeLa: 0.5 mL
10. Add new preheated cell culture medium up to 5 mL to inactivate the trypsin activity.
11. Measure the concentration of cells per mL in the cell suspension by using a coulter counter. At least two measurements should be performed on each of the three parallels.
12. Calculate the mean total number of cells and standard deviation for each treatment.
13. Repeat step 7-12 every day until confluence is reached.

Appendix 7: ***Protocol for seeding out cells for clonogenic assay***

1. Irradiate the cells with the desired radiation dose.
2. Heat cell culturing medium, PBS and trypsin in a heat bath until the temperature is about 37 °C.
3. Remove medium from the cells and wash with PBS.
4. Add trypsin to detach the cells
5. Inactivate the trypsin by adding 5 mL medium to each well.
6. Transfer the cell suspensions to 15 mL-tubes and add medium up to 10 mL (4.5 mL to HeLa; 4 mL to SiHa). Mix thoroughly.
7. Use 6 mL for counting the number of cells per mL.
8. Calculate how much medium is needed to be added to each cell suspension in order to obtain the desired concentration of cells.

Radiation dose	Number of cells to be plated	Concentration
0	300	1 cell/µL
2	1000	3.3 cells/µL
4	10 000	33.3 cells/µL

9. Add 300 µL of the diluted cell suspension to three wells. Fill up with 2 mL cell medium

Appendix 8: ***Protocol for fixating and staining colonies***

Fixation (in fume hood)

1. Remove cell medium.
2. Add 1-2 mL ice cold methanol, wait for 2-3 min before removing it. Let the dishes air dry in the fume hood.

Staining (on bench)

3. Add 1-2 mL 0.05 % crystal violet to each well and leave for a couple of minutes.
4. Remove excessive staining.
5. Wash the dishes in a Styrofoam box filled with water.
6. Air dry the dishes on the bench over night.

Appendix 9: ***Protocol for freezing cells (for flow cytometry)***

1. Heat cell medium, PBS and trypsin until the temperature is about 37 °C

In LAF bench

2. Remove medium from the cells
3. Wash the cells in each well with 1 mL PBS
4. Add trypsin to each well to detach the cells
    - HeLa: 0.5 mL
    - SiHa: 1 mL
5. Neutralize by adding 2 mL pre-heated medium to each well
6. Transfer each of the cell suspensions to flow tubes and centrifuge at 1000 rpm for 5 min.
7. Remove supernatant
8. Add 1 mL methanol and dissolve the pellet
9. Store the tubes at -20°C

Appendix 10: ***Preparing cells for TUNEL assay and Hoechst staining***

1. Withdraw the methanol-fixated cells from the -20°C freezer
2. Add 3 mL PBS to each sample
3. Centrifuge the samples at 1700 rpm for 3 min and remove the supernatant.
4. Make the reaction mix for the selected number of samples.
   Volumes of <u>one reaction</u>:

Solution	**Volume (µL)**
TdT enzyme	0.16
TdT Reaction Buffer	4.00
$CoCl_2$ (25mM)	2.40
Biotin-16-dUTP	0.40
DTT (10mM)	0.40
=	7.36
+ ddH_2O	32.64
Total volume	*40*

5. Resuspend the cells from one sample in 40 µL reaction mix solution. Vortex and incubate the cells for 30 min 37°C to allow the TdT enzyme to work.
6. Make a 5 % (w/v) dry milk (fat free) suspension in PBS. Mix thoroughly and centrifuge at 1700 rpm for 3 min. Keep the supernatant for later steps.
7. Add 3 mL PBS to each sample.
8. Centrifuge the cells at 1700 rpm for 3 min and remove supernatant.
9. Resuspend the cells in 70 µL 5 % dry milk suspension containing the fluorochrome-labeled streptavidin in 1:400 dilution of Streptavidin-Cy5 (50-100µl solution should be used per sample). Vortex and incubate the cells for 30 min at room temperature protected from light.
10. Add 3 mL PBS to each sample
11. Centrifuge the cells at 1700 rpm for 3 min and remove supernatant.
12. Dilute Hoechst 33258 with PBS into a final dilution of 1.5 µg/mL.
    Volumes for <u>one sample</u>:

Hoechst 33258 (624 µg/mL)	**PBS**
1.2 µL	0.5 mL

13. Add 500 µL of 1.5 µg/mL Hoechst to each tube

Wait for at least 30 minutes before filtering the samples. Filtration is done to avoid clumps of cells. The samples are now ready for analysis.

Appendix 11: ***Calculated upregulation of miR-320d – raw data***

	Upregulation of miR-320d* (relative to negative control)	
Experiment	*SiHa*	*HeLa*
1	30630	6361
2	17912	17388
3	7923	8909
Average	18821	10886
St.dev	11381	5773

*Raw data from each of three transfection experiments performed on SiHa and HeLa cells. Calculated by using the $2^{-\Delta\Delta Ct}$ method.

	miR-320d upregulation** (relative to negative control)	
Day	*SiHa*	*HeLa*
0	30630	6361
1	1249	1593
2	975	705
3	1022	1054
4	536	382
5	-	178
6	473	-
7	184	88
8	215	101
9	-	42
10	79	85
11	107	-
12	43	-

**Raw data from transfection duration-experiment. The experiment is based on cell seeded out from transfection experiment 1, but day 0 is excluded due to different conditions before harvest.

Appendix 12: ***Numbers of cells from proliferation assay – raw data***

Number of cells (average from three flasks)*

	SiHa		HeLa	
Day	*Neg. control*	*Mimic*	*Neg. control*	*Mimic*
0	50 000	50 000	50 000	50 000
1	58 283	60 783	63 640	64 183
2	-	-	113 830	94 537
3	195 983	135 917	197 977	174 950
4	341 500	293 983	-	-
5	-	-	992 833	1 003 417
6	1199 833	974 667	2 258 767	2 360 433
7	1 742 833	1 126 167	3 358 600	3 486 000
8	3 262 667	2 765 000	4 680 600	4 766 600
9	4 909 000	4 094 833	5 101 667	5 035 667
10	6 304 167	5 881 667	-	-

*Numbers of cells counted over a period of 10 days (SiHa) and 9 days (HeLa)

Appendix 13: ***Raw data on cell survival***

Average plating efficiency (%, from three wells)*

	SiHa		HeLa	
Experiment	*Neg. control*	*Mimic*	*Neg. control*	*Mimic*
1	39.5	29.8	32.0	14.8
2	29.2	22.1	27.7	23.4
3	39.3	31.6	20.8	13.1
Average	36.0	27.8	26.8	17.1
St.dev	5.9	5.1	5.6	5.5

* Clonogenic survival shown as plating efficiency for three individual experiments on SiHa and HeLa cells

Appendix 14: ***Cell cycle distribution - raw data***

SiHa

Normalized cell cycle distributions (%)*

	G1		S		G2/M	
Experiment	*Neg. control*	*Mimic*	*Neg. control*	*Mimic*	*Neg. control*	*Mimic*
1	67.5	64.8	23.2	22.5	9.3	12.7
2	50.4	62	38.4	28.3	11.2	9.7
3	60.9	57.4	26.6	31.6	10.4	12.3
Average	59.6	61.4	29.4	27.5	10.3	11.6
St.dev	8.6	3.7	8.0	4.6	1.0	1.6

HeLa

Normalized cell cycle distributions (%)*

	G1		S		G2/M	
Experiment	*Neg. control*	*Mimic*	*Neg. control*	*Mimic*	*Neg. control*	*Mimic*
1	47.3	47.2	38.0	34.1	14.7	18.7
2	48.0	46.8	42.2	39.2	9.8	14.0
3	46.4	46.3	31.2	33.9	12.2	18.3
Average	47.2	46.8	37.1	35.7	12.2	17.0
St. dev	0.8	0.4	5.5	3.0	2.5	2.6

* Cell cycle distributions from three individual experiments on SiHa and HeLa cells, normalized in order to make the sum of all cell cycle phases 100 %.

Appendix 15: ***Apoptosis – raw data from TUNEL assay***

	Fraction of non-apoptotic cells (%)*			
	SiHa		HeLa	
Experiment	*Negative control*	*Mimic*	*Negative control*	*Mimic*
1	99.6	99.7	98.2	99.2
2	99.7	99.9	98.1	*97.4*
3	96.8	97.2	-	-
Average	98.7	98.9	98.2	98.3
St.dev	1.6	1.5	0.1	1.3

Fraction of non-apoptotic cells (%)*	
Reh positive control	72.4

* Apoptotic fractions of three individual experiments on SiHa cells, two experiments on HeLa cells and in addition Reh cells as positive control

Appendix 16: ***Raw data on radiosensitivity***

SiHa

Average plating efficiency (%, from three wells)**

	0 Gy		**2 Gy**		**4 Gy**	
Experiment	*Neg. control*	*Mimic*	*Neg. control*	*Mimic*	*Neg. control*	*Mimic*
1	24.9	22.6	5.0	4.9	2.8	2.2
2	33.7	32.1	4.5	5.0	3.0	2.1
3	42.7	40.1	12.0	12.4	1.7	1.5

HeLa

Average plating efficiency (%, from three wells)**

	0 Gy		**2 Gy**		**4 Gy**	
Experiment	*Neg. control*	*Mimic*	*Neg. control*	*Mimic*	*Neg. control*	*Mimic*
1	22.9	11.6	7.6	2.7	0.9	0.7
2	22.9	22.8	7.6	5.8	2.1	1.7
3	26.1	23.3	8.9	5.4	1.8	0.8

** Clonogenic survival after irradiation, shown as plating efficiency, and used for studying radiosensitivity

Appendix 17: ***Materials***

Reagents

Name	Company	Catalog number
Biotin-16-dUTP	Roche	11093070910
Chloroform	Merck Millipore	1024452500
Crystal violet NAF 0.5 %	Apotek 1	327973
DharmaFECT 1 Transfection Reagent	GE Healthcare Dharmacon Inc.	T-2001-03
DL-Dithiothreitol solution	Sigma-Aldrich	646563
Dulbecco's Modified Eagles Medium (DMEM)	ThermoFisher Scientific	31966-047
Dulbecco's Phosphate Buffered Saline (PBS)	Sigma-Aldrich	D8537
ExiLENT SYBR® Green master mix, 20ml	Exiqon	203421
Fetal bovine serum (FBS)	ThermoFisher Scientific	16000044
Hoechst 33258	Sigma-Aldrich	861405
hsa-miR-103a-3p LNA™ PCR primer set, UniRT	Exiqon	204063
hsa-miR-320d LNA™ PCR primer set, UniRT	Exiqon	205667
L-glutamine (LG)	Sigma-Aldrich	G7513
Methanol	VWR	20864.320
miRIDIAN microRNA Human hsa-miR-320d – Mimic	GE Healthcare Dharmacon Inc.	C-301440-00-005
miRIDIAN microRNA Mimic Negative Control #1	GE Healthcare Dharmacon Inc.	CN-001000-01-05
miRNeasy Mini Kit	Qiagen	217004
NaCl, 0.9 %	B. Braun	
Nuclease-free water	ThermoFisher Scientific	AM9932
QIAzol lysis reagent	Qiagen	79306
Reference Dye for Quantitative PCR (ROX)	Sigma-Aldrich	R4526-.3ML
5x siRNA buffer	GE Healthcare Dharmacon Inc.	B-002000-UB-100
Streptavidin	Ge Healthcare	PA92005
TdT Kit containing $CoCl_2$, TdT enzyme and TdT reaction buffer	Sigma-Aldrich	03333574001
Trypsin-EDTA	Sigma-Aldrich	T3924
Universal cDNA Synthesis Kit II	Exiqon	203301

Equipment

Name	Company	Catalog Number
6-well plates	ThermoFisher Scientific	14-832-11
T75 flasks	ThermoFisher Scientific	156499
T25 flasks	ThermoFisher Scientific	146516
Cell culture dishes 35 mm	Becton Dickinson	358001
Cell scraper, 16 cm	Sarstedt	83.1832
MicroAmp® Fast Optical 96-Well Plate	ThermoFisher Scientific	4346906
MicroAmp® Optical Adhesive Film	ThermoFisher Scientific	4311971

Instruments

Name	Company
ABI 7900HT Fast Real-Time	Applied Biosystems
GeneAmp® PCR System 9700	Applied Biosystems
BD LSR II – Flow cytometer	BD Biosciences
Beckman counter Z2	Beckman Coulter Life Sciences
NanoDrop 2000 Spectrophotometer	ThermoFisher Scientific
Faxitron CP160	Faxitron Bioptics
Core facilities:	
Agilent 2200 TapeStation	Aligent Technologies

Software

Name	Developer
FlowJo V7.6.5	TreeStar
SDS V2.3	Applied Biosystems